N-1851

NCEL
Technical Note

January 1993
By George Warren and
Ronald Shope

Sponsored By Office of Chief of
Naval Research

IMPACT LOAD METHOD FOR STRUCTURAL ASSESSMENT OF PIERS AND BRIDGES

ABSTRACT NCEL examined the Impact Load Method (ILM) to elicit a response from bridges and piers as a means of structural assessment. Stiffness changes were detected that were correlated to loss of structural function from material damage and deterioration. Parametric studies were performed on a one-third scale model pier and a highway bridge using finite element modeling that was verified by ILM tests. Studies showed that the ILM is sensitive to the loss of cross section in pier and bridge decks and well as to the loss of pile support.

NAVAL CIVIL ENGINEERING LABORATORY PORT HUENEME CALIFORNIA 93043-4328

METRIC CONVERSION FACTORS

Approximate Conversions to Metric Measures

Symbol	When You Know	Multiply by	To Find	Symbol
		LENGTH		
in	inches	*2.5	centimeters	cm
ft	feet	30	centimeters	cm
yd	yards	0.9	meters	m
mi	miles	1.6	kilometers	km
		AREA		
in^2	square inches	6.5	square centimeters	cm^2
ft^2	square feet	0.09	square meters	m^2
yd^2	square yards	0.8	square meters	m^2
mi^2	square miles	2.6	square kilometers	km^2
	acres	0.4	hectares	ha
		MASS (weight)		
oz	ounces	28	grams	g
lb	pounds	0.45	kilograms	kg
	short tons (2,000 lb)	0.9	tonnes	t
		VOLUME		
tsp	teaspoons	5	milliliters	ml
Tbsp	tablespoons	15	milliliters	ml
fl oz	fluid ounces	30	milliliters	ml
c	cups	0.24	liters	l
pt	pints	0.47	liters	l
qt	quarts	0.95	liters	l
gal	gallons	3.8	liters	l
ft^3	cubic feet	0.03	cubic meters	m^3
yd^3	cubic yards	0.76	cubic meters	m^3
		TEMPERATURE (exact)		
°F	Fahrenheit temperature	5/9 (after subtracting 32)	Celsius temperature	°C

*1 in = 2.54 (exactly). For other exact conversions and more detailed tables, see NBS Misc. Publ. 286, Units of Weights and Measures, Price $2.25, SD Catalog No. C13.10:286.

Approximate Conversions from Metric Measures

Symbol	When You Know	Multiply by	To Find	Symbol
		LENGTH		
mm	millimeters	0.04	inches	in
cm	centimeters	0.4	inches	in
m	meters	3.3	feet	ft
m	meters	1.1	yards	yd
km	kilometers	0.6	miles	mi
		AREA		
cm^2	square centimeters	0.16	square inches	in^2
m^2	square meters	1.2	square yards	yd^2
km^2	square kilometers	0.4	square miles	mi^2
ha	hectares (10,000 m^2)	2.5	acres	
		MASS (weight)		
g	grams	0.035	ounces	oz
kg	kilograms	2.2	pounds	lb
t	tonnes (1,000 kg)	1.1	short tons	
		VOLUME		
ml	milliliters	0.03	fluid ounces	fl oz
l	liters	2.1	pints	pt
l	liters	1.06	quarts	qt
l	liters	0.26	gallons	gal
m^3	cubic meters	35	cubic feet	ft^3
m^3	cubic meters	1.3	cubic yards	yd^3
		TEMPERATURE (exact)		
°C	Celsius temperature	9/5 (then add 32)	Fahrenheit temperature	°F

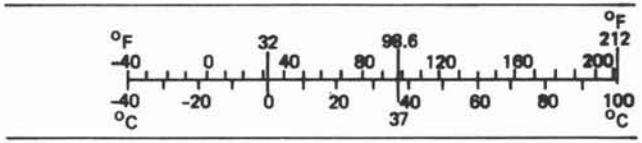

REPORT DOCUMENTATION PAGE

Form Approved
OMB No. 0704-018

1. AGENCY USE ONLY *(Leave blank)*	2. REPORT DATE	3. REPORT TYPE AND DATES COVERED
	January 1993	Not final: June 1991 through June 1992

4. TITLE AND SUBTITLE

IMPACT LOAD METHOD FOR STRUCTURAL ASSESSMENT OF PIERS AND BRIDGES

5. FUNDING NUMBERS

PR - RM33F60A899020
WU - DN044010

6. AUTHOR(S)

George Warren and Ronald Shope

7. PERFORMING ORGANIZATION NAME(S) AND ADDRESS(S)

Naval Civil Engineering Laboratory
Port Hueneme, CA 93043-4328

8. PERFORMING ORGANIZATION REPORT NUMBER

TN-1851

9. SPONSORING/MONITORING AGENCY NAME(S) AND ADDRESS(S)

Office of the Chief of Naval Research
Office of Naval Technology
Arlington, VA 22217-5000

10. SPONSORING/MONITORING AGENCY REPORT NUMBER

11. SUPPLEMENTARY NOTES

12a. DISTRIBUTION/AVAILABILITY STATEMENT

Approved for public release; distribution is unlimited.

12b. DISTRIBUTION CODE

13. ABSTRACT *(Maximum 200 words)*

NCEL examined the Impact Load Method (ILM) to elicit a response from bridges and piers as a means of structural assessment. Stiffness changes were detected that were correlated to loss of structural function from material damage and deterioration. Parametric studies were performed on a one-third scale model pier and a highway bridge using finite element modeling that was verified by ILM tests. Studies showed that the ILM is sensitive to the loss of cross section in pier and bridge decks and well as to the loss of pile support.

14. SUBJECT TERMS

Impact load method, finite element method, bridges, piers, reinforced concrete

15. NUMBER OF PAGES

67

16. PRICE CODE

17. SECURITY CLASSIFICATION OF REPORT	18. SECURITY CLASSIFICATION OF THIS PAGE	19. SECURITY CLASSIFICATION OF ABSTRACT	20. LIMITATION OF ABSTRACT
Unclassified	Unclassified	Unclassified	UL

CONTENTS

INTRODUCTION

Insuring the continued safe use of Navy piers and bridges requires a method of assessing their structural condition in an efficient and timely manner. The method must be capable of not only locating damaged or deteriorated areas, but also providing the necessary information to deduce the load capacity of the structure.

The purpose of this study was to examine the Impact Load Method (ILM) as a means of performing structural assessment on Navy piers and bridges. The basis for this method is the assumption that a loss in effective cross section due to damage or deterioration can be correlated to a reduction in the stiffness of the structure. This stiffness reduction is detected by applying impact loads to the structure and comparing the displacement responses of identical, "ideal" spans or comparing the test results to the results obtained from finite element analyses.

The specific objectives were to examine the behavior of structures subjected to impact load tests and determine the sensitivity of the impact load method in detecting stiffness changes in pier and bridge structures. Two structures were considered, each with a different type of damage. The first was a one-third scale pier model. This model was used to examine the sensitivity of detecting damage caused by overload in a reinforced concrete deck. The second structure was a highway bridge at Naval Weapons Station (WPNSTA), Earle, New Jersey. This structure was used to examine the sensitivity of the method for detecting damage or deterioration in timber pile supports.

The nondestructive evaluation (NDE) approach using the ILM was as follows:

1. Perform ILM survey on all areas (damaged and undamaged) of each structure.

2. Compare the displacement responses of damaged and undamaged areas.

3. Use the results of the undamaged areas to calibrate a finite element model of each structure.

4. Develop a rational method of representing the damage in the finite element model based on section loss. Test the method with the experimental response of the damaged areas.

5. Use the method of modeling damage to conduct a parameter study of the sensitivity to stiffness changes in the structures.

6. Test the response of the damaged finite element model with the experimental (ILM) response.

correlated to loss of effective areas in concrete and steel, loss of support, and other damage and deterioration.

APPLICATION OF ILM

Apparatus

ILM tests were performed using the Falling Weight Deflectometer (FWD) shown in Figures 1 and 2. The FWD is a computer-controlled trailer-mounted device that applies impact loads to the surface of the deck and records load and displacement time histories. A system (not including a tow vehicle) can be procured at a cost ranging from $100K to $120K. The loads are generated by releasing a mass from a height and allowing it to drop onto an elastomeric spring system. This produces a load pulse with a duration of 25 to 35 milliseconds (msec) (Ref 15). The springs extend the load duration and generate a load pulse that approximates a half sine wave. By adjusting the weight of the mass, the drop height, or both, the FWD can produce peak loads ranging from 6.5 to 54 kips. The weight of the mass ranges from 440 to 1,540 pounds and the drop height ranges from 1 to 16 inches. The load is uniformly distributed by a 12-inch-diameter steel plate padded with 1 inch of an elastomeric material (Ref 16).

The displacements are obtained by measuring and integrating output from velocity gages (geophones). This integration is performed by the FWD system processor. One of the geophones is located at the center of the load plate and six to eight additional geophones are attached to a support bar and can be located from 8 inches to 8 feet from the center of the load plate. The loads are measured by a load cell located directly below the falling mass. The load and displacement readings are digitized at 0.2-msec intervals over a 60-msec time period after each drop.

The FWD system processor digitizes electrical analog signals from the transducers and performs data reduction in real time. Peak load and displacement values are retrieved from the time history records by a computer inside the tow vehicle and displayed immediately on a monitor. Hard copies of peak values are printed out shortly after they are displayed on the monitor. Time histories are stored on a floppy disk in a format that is compatible with spreadsheet programs such as Lotus 1-2-3. The spreadsheet program provides further data conditioning, calculation, and plotting.

Procedure

The test sequence is controlled by computer. The operator inputs the selected mass and the drop heights to the operating software. The load plate is positioned directly over the test point and lowered along with the displacement sensors to the surface of the deck. The actual test sequence is preceded by a seating drop of 1 to 2 inches. This is to ensure that the sensors and load plate are in good contact with the deck. After the seating load, the FWD hydraulically lifts the mass to the programmed height and releases it. The system processor digitizes and records either the peak values of the load and displacements or the entire load and displacement histories as specified by the operator. After the measurements are recorded for the last drop, the load plate assembly is hydraulically lifted off of the deck and positioned so that the trailer can be moved freely. The FWD is then moved to the next test point and the procedure is repeated.

Figure 1
Falling weight deflectometer and tow vehicle.

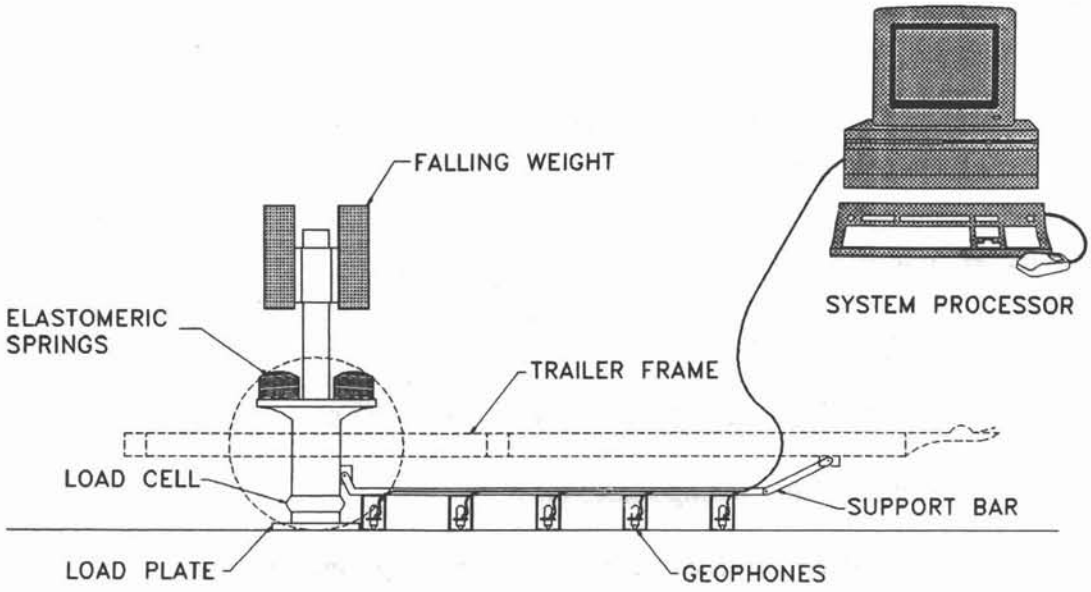

Figure 2
Falling weight deflectometer system.

Impact Load Characteristics

The following assumptions were made in examining the impact load generated by the FWD:

- The mass fell freely onto the springs and no friction existed between the mass and the guide system.
- The springs, steel plate, and elastomeric pad could be represented by a single equivalent linear elastic spring with a constant stiffness.
- The impact between the falling mass and the springs was a perfectly elastic collision and the total kinetic energy of the mass an instant before impact was equal to the total kinetic energy of the system after the collision.
- Internal damping of the FWD apparatus could be neglected.
- The mass of the springs, steel plate, and rubber pad could be neglected.

The FWD apparatus can then be represented by the discrete mass-spring model shown in Figure 3. The mass is released and strikes the top of the spring at time t_o. As the spring compresses, the structure begins to displace downward relieving the force in the spring. Therefore, the force the FWD imparts is actually a function of the mass and stiffness of the structure as well as the FWD mass and drop height. To examine this force, it is necessary to consider the case in which impact load tests are performed on a nondeforming surface.

Assuming that point B in Figure 3 is fixed, the total downward displacement of point A after time $t = t_o$ is given by the following equation (Ref 15):

$$y(t) = \frac{v_o}{\omega} \sin \omega t + \frac{W_m}{K} (1 - \cos \omega t) \qquad (1)$$

where $y(t)$ = downward displacement at point A, inches

v_o = velocity of mass at $t = t_o$, in./sec

ω = natural frequency of oscillation of the FWD system, hertz

W_m = weight of the falling mass, kips

K = equivalent spring constant of the FWD system, kips/in.

t = time elapsed from impact, seconds

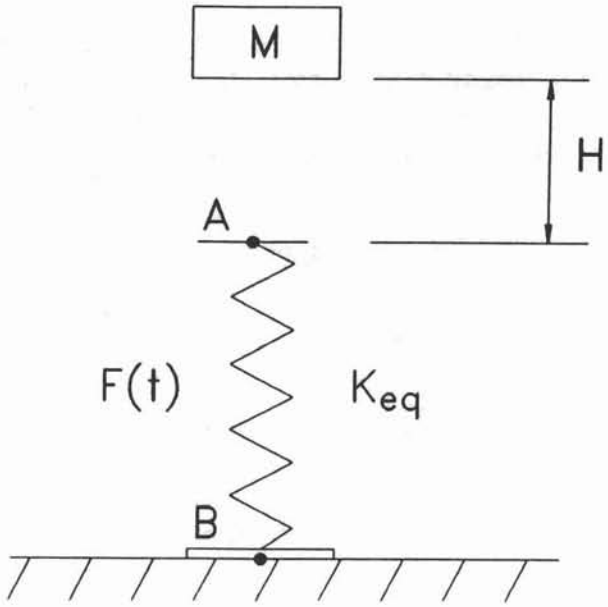

Figure 3
FWD single-degree-of-freedom mass-spring model.

The velocity of the mass at impact, v_o, is given by the following equation:

$$v_o = \sqrt{2gH} \tag{2}$$

where g = acceleration due to gravity, in./sec^2

H = drop height of mass, inches

The natural frequency of the FWD system, ω, is defined as:

$$\omega = \sqrt{\frac{K}{M}} \tag{3}$$

where M = falling mass, kip-sec^2/in. Equation 1 can be written as follows:

$$y(t) = \left[\frac{2\,g\,HM}{K}\right]^{1/2} \sin\,\omega t + \frac{W_m}{K}\,(1-\cos\,\omega t) \qquad (4)$$

The second term in the equation represents the displacement at point A caused by the dead weight of the mass. For drop heights ranging from 8 to 14 inches, this term accounts for less than 3 percent of the total displacement. Therefore, it can be ignored and the equation for the downward displacement at point A essentially becomes:

$$y(t) = \left[\frac{2\,g\,HM}{K}\right]^{1/2} \sin\,\omega t \qquad (4a)$$

The force the FWD imparts to the structure at point B is determined by the following relationship:

$$F(t) = K\,y(t)$$

Therefore, the equation for the load as a function of time is as follows:

$$F(t) = (2\,g\,HMK)^{1/2} \sin\,\omega t \qquad (5)$$

Equation 5 is valid for impact load tests on nondeformable structures for the range of time in which the falling mass is in contact with the springs and the springs are in compression, that is, $0 < t < \pi/\omega$.

Equation 5 is useful for experimentally determining the equivalent stiffness of the test apparatus. From Equation 5, the peak load occurs at time $t = \pi/2\omega$ and is given by the following equation:

$$F_{max} = (2\,g\,HMK)^{1/2} \qquad (6)$$

The mass and the drop height are known and F_{max} is measured by the load cell positioned beneath the falling weight. The only unknown is the equivalent stiffness, K, of the FWD. By selecting a test point that experiences very small displacements, such as over a bridge abutment, the equivalent stiffness of the FWD apparatus can be determined.

Tests have shown that the equivalent stiffness, K, increases as the mass or drop height increases. This increase can be attributed to the material nonlinearity of the elastomeric springs and the geometric changes in the cross section of the springs as deformation occurs. Therefore, if a constant equivalent stiffness is used, it must be determined experimentally for each mass and drop height combination.

NCEL MODEL PIER TESTS

Pier Description

The NCEL pier model, shown in Figure 4, was a five-span reinforced concrete deck with pile cap supports at 6-foot intervals. The model was a one-third scale reproduction of a pier deck and was reinforced as a one-way slab with two layers of reinforcing steel in both directions. D5 deformed wire (equivalent to a No. 2 deformed, grade 60 bar) and No. 3 deformed, grade 60 bars were used with 4,000-psi (design compressive strength) concrete. The clear span of the deck was 5 feet and the slab thickness was 5-3/8 inches. The pier model was built for a Naval Facilities Engineering Command (NAVFAC) Engineering Investigation (EI) project to measure load distribution and failure modes for crane outrigger pads (Ref 17).

Figure 5 shows a section view of a typical interior span. Transverse reinforcement parallel to the supports remained constant throughout the deck except for the end spans. The flexural reinforcement perpendicular to the supports varied depending on whether the design moment for the given section was positive or negative. The cap beams were supported by the 2-foot-thick floor of the test building. Reference 17 contains a complete description of the NCEL pier.

The concrete strength was determined from cylinder tests in accordance with ASTM C469-87a (Ref 18). The cylinder strength was 7,500 psi for the spans under consideration. The measured modulus of elasticity was 4,020 ksi.

Coupon tests of the reinforcing steel were conducted in accordance with ASTM E8-87 (Ref 19). The No. 2 bars had a yield strength of 81,000 psi and an ultimate strength of 85,000 psi. The No. 3 bars had a yield strength of 69,000 psi and an ultimate strength of 109,000 psi.

Prior to conducting the ILM tests, the center span was subjected to cyclic load (patch load) and a single monotonic load which exceeded the ultimate capacity of the deck. Damage (excessive deformation, large cracks, and deformed steel) was observed in the immediate area of the load. Cracks formed concentric circles around the load point on the deck top and radiated from the load point on the deck bottom. The mode of failure was punching shear. Figure 6 shows the location of the patch load and the extent of the visible damage. No damage existed in the adjacent spans.

ILM Tests

Setup. Figure 7 shows the location of the three selected test points. Test point 1 was on the undamaged span, test point 2 was at the corresponding location on the damaged span, and test point 3 was on the damaged span closer to the boundary of the observed cracks. The displacement sensors were positioned transversely along the midspan.

Based on calibration tests, NCEL selected a mass weighing 880 pounds with a maximum drop height of 14 inches to produce a measurable deflection response well within the elastic limit of the structure. Two drop heights (8.375 and 14 inches) were used to check linearity between load and deflection while the weight of the falling mass (880 pounds) remained constant. Two tests were performed for each drop height to check system repeatability. Only peak loads measured by the load cell and maximum deflections measured at the seven sensor locations were recorded.

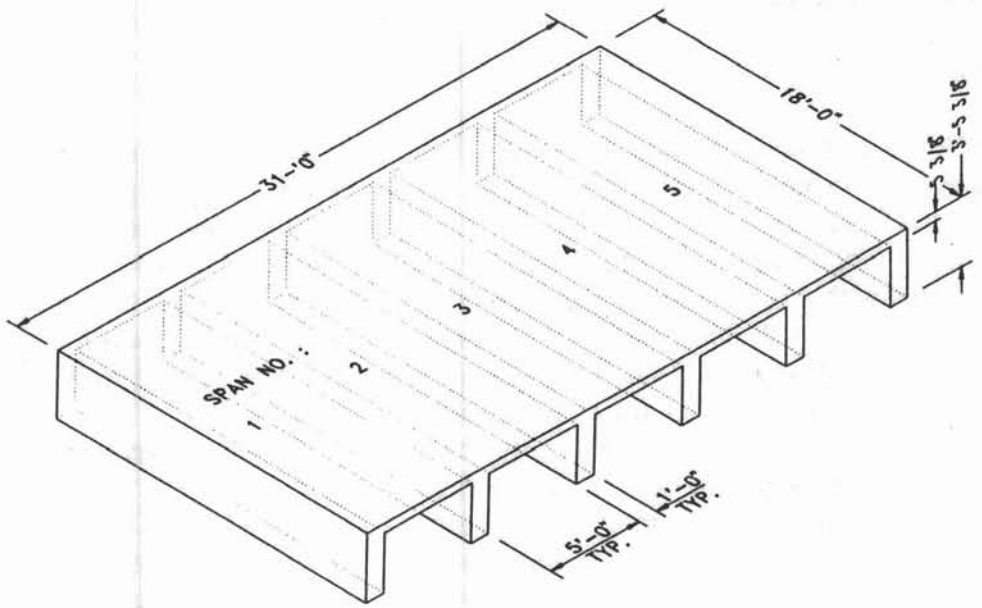

Figure 4
NCEL model pier.

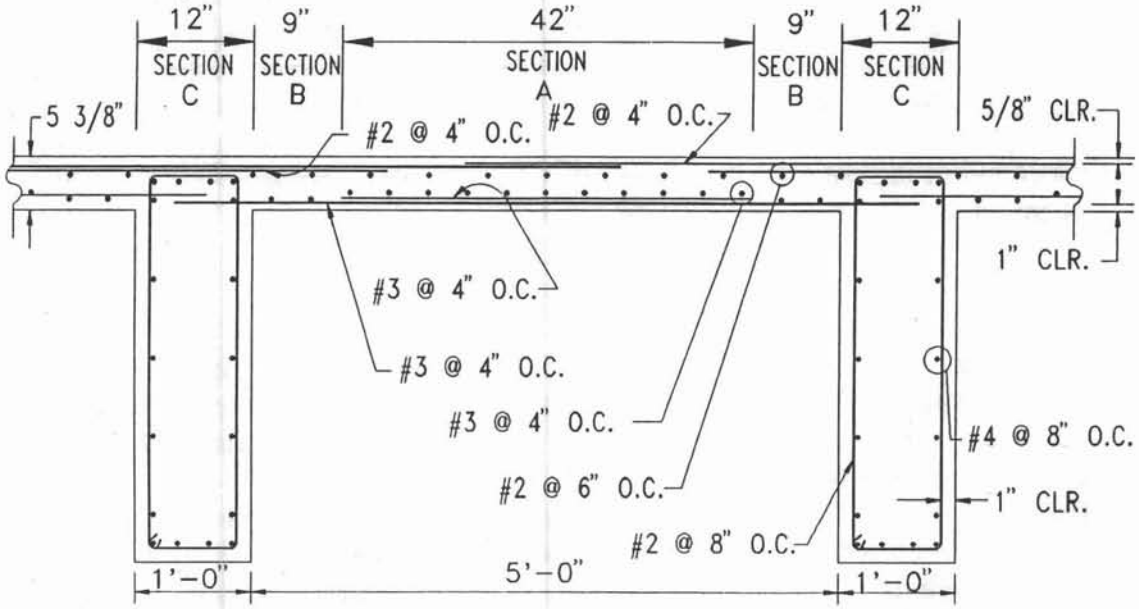

Figure 5
Section view of typical interior span.

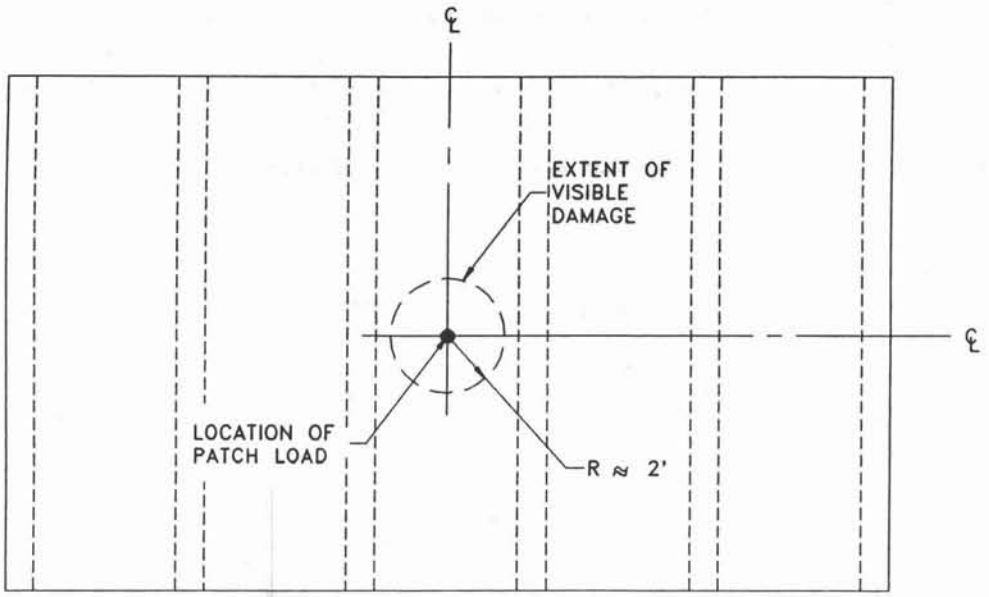

Figure 6
Plan view showing location of patch load and extent of damage.

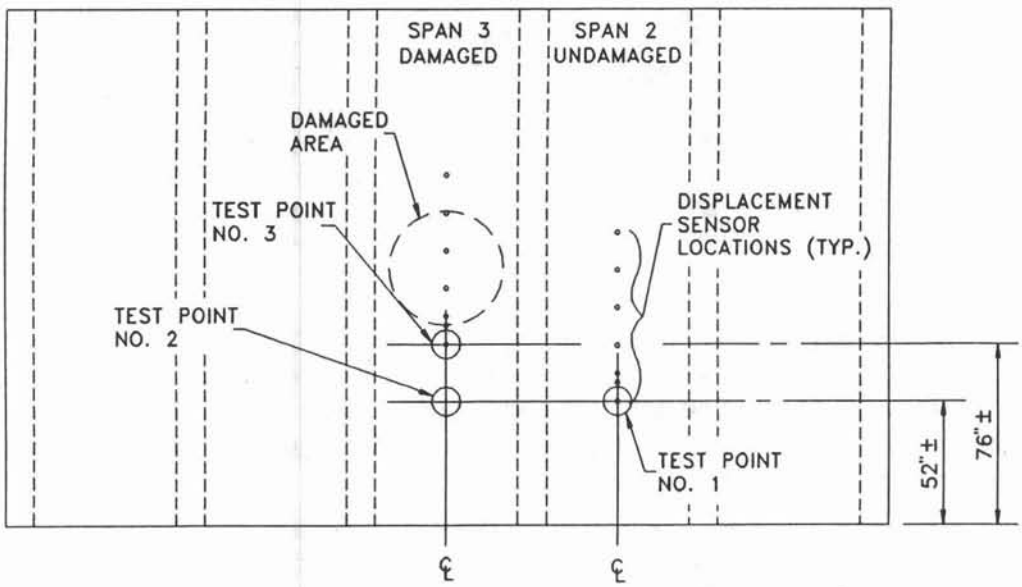

Figure 7
Plan view showing test point locations and displacement sensor locations.

Test Results. Table 1 gives the results of the ILM tests. The maximum variation of peak load measurements for any two identical tests occurred for the 8.375-inch drop height at test point 1. The two recorded values (19.63 and 19.75) differed by 0.6 percent. The maximum variation in deflection measurements occurred for the 8.375-inch drop height at test point 2. Five of the sensors recorded values that varied by approximately 5 percent with the maximum of 5.3 percent occurring at the sensor located 55 inches from the load. The FWD produced consistent results for both applied loads and measured displacements.

Table 1
ILM Test Results For NCEL Pier

Test Pt.	Drop Height (in.)	Peak Load (kips)	Maximum Deflection (mils) for Sensor Location (in.)						
			0	8	12	24	39	55	71
1	8.375	19.63	19.62	17.35	15.32	10.51	5.81	3.17	2.09
1	8.375	19.75	19.68	17.39	15.35	10.52	5.82	3.16	2.11
1	14.00	28.11	27.97	24.73	21.87	14.94	8.28	4.58	2.72
1	14.00	28.06	27.98	24.72	21.86	14.93	8.29	4.56	2.72
2	8.375	19.63	21.83	20.27	18.59	14.04	9.38	11.44	3.93
2	8.375	19.59	20.74	19.28	17.76	13.51	8.96	10.86	3.82
2	14.00	28.13	30.11	28.05	25.78	19.28	12.65	11.89	4.96
2	14.00	27.99	29.85	27.78	25.48	19.04	12.65	11.87	4.98
3	8.375	20.98	33.81	34.92	34.00	29.67	10.57	6.04	3.79
3	8.375	20.91	33.25	34.31	33.41	29.19	10.63	6.11	3.86
3	14.00	29.35	47.42	48.56	47.48	41.36	15.44	8.94	4.81
3	14.00	29.39	47.74	48.80	47.69	41.53	15.69	9.11	4.93

In Figures 8 through 12, each graph represents the average results of the two identical tests. Figure 8 shows the peak deflection response at each sensor location for test point 1 (undamaged span) to both drop heights. The deflection graphs smoothly decay away from the point of load with no abrupt changes in slope. The displacements for the 14-inch drop height increased in proportion to the peak loads.

Figure 9 shows the test results for test point 2 (damaged span). The location of the maximum damage and the extent of the visible damage are superimposed on the graph. The figure shows that changes in the slope of both graphs occur near the boundary of the visible damage (38 inches from the load point) and at the point of maximum damage (57 inches from the load point). The figure also shows that the displacements at the point of damage did not increase linearly with load. This suggests that either an error in the displacement measurements occurred or the structure exhibited nonlinear behavior in the damaged area. NCEL suspects the latter due to the extent of the damage.

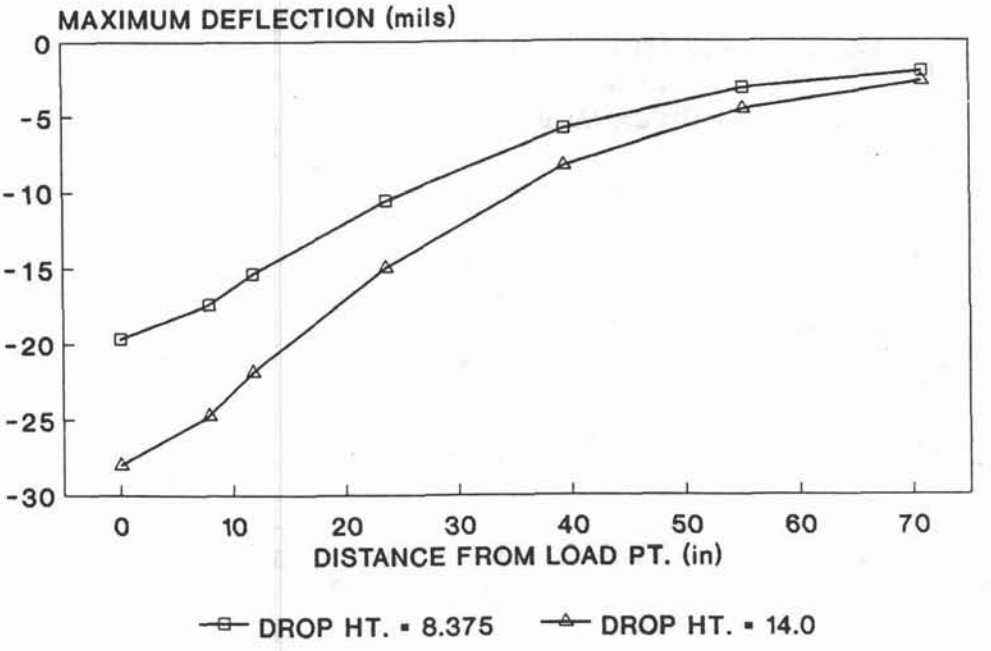

Figure 8
ILM results for test point no. 1 (undamaged span).

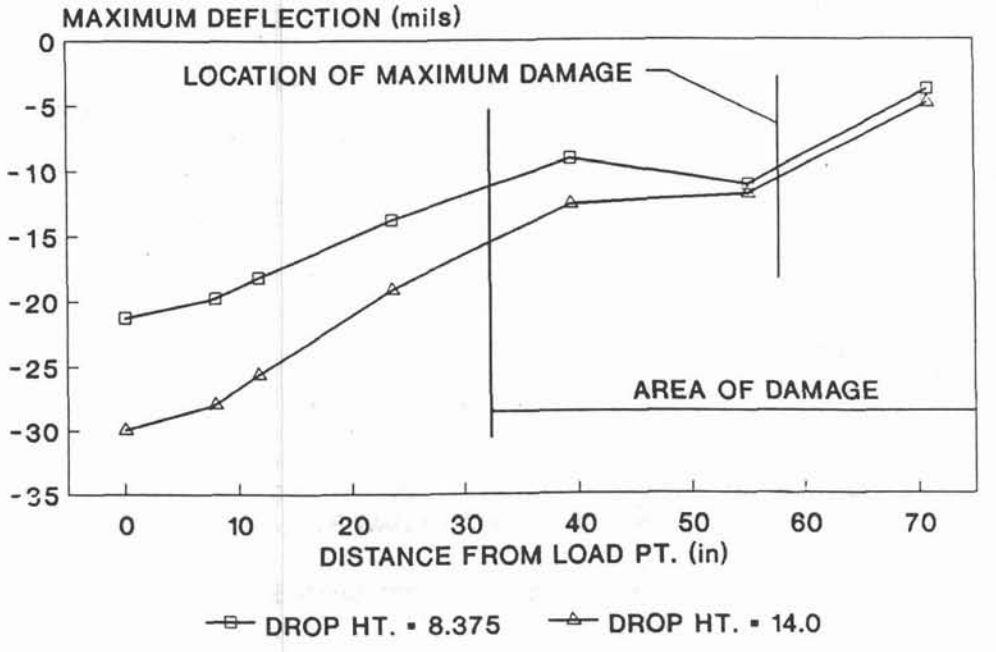

Figure 9
ILM results for test point no. 2 (damaged span).

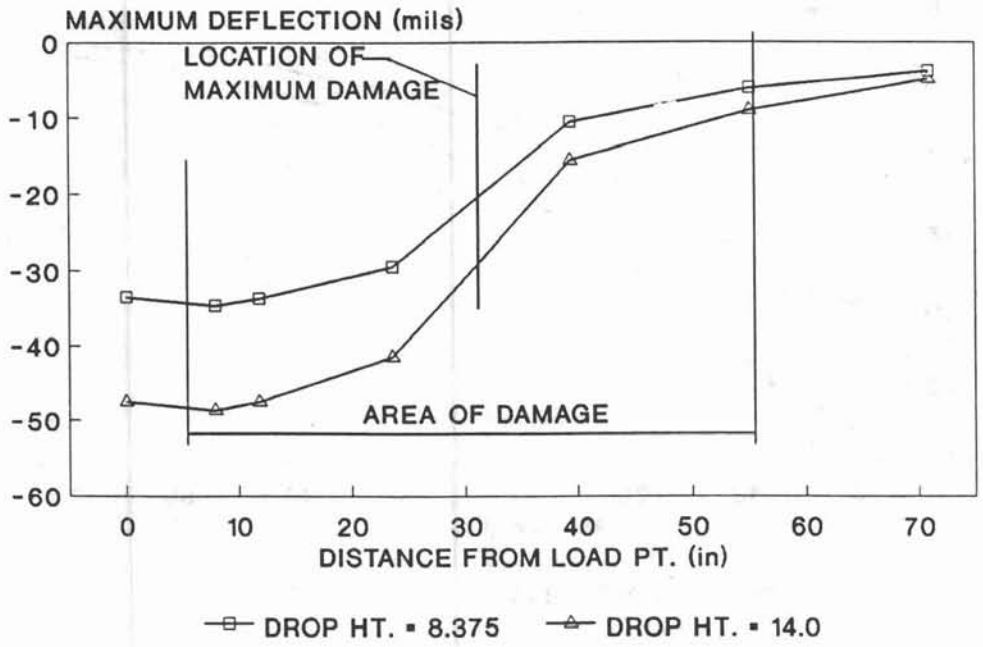

Figure 10
ILM results for test point no. 3 (damaged span).

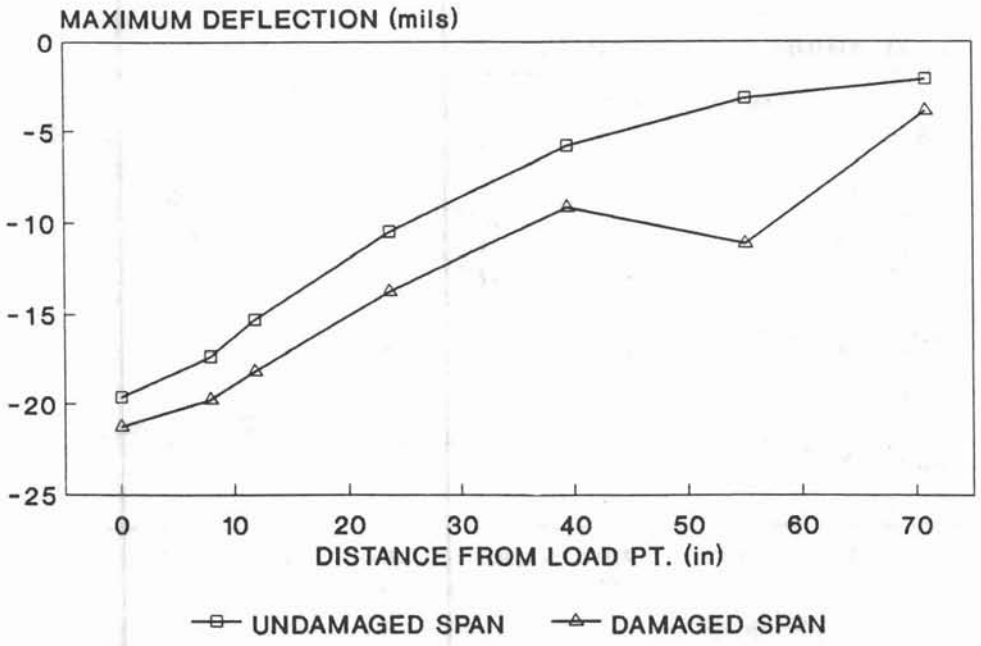

Figure 11
ILM results for damaged and undamaged span drop height = 8.375.

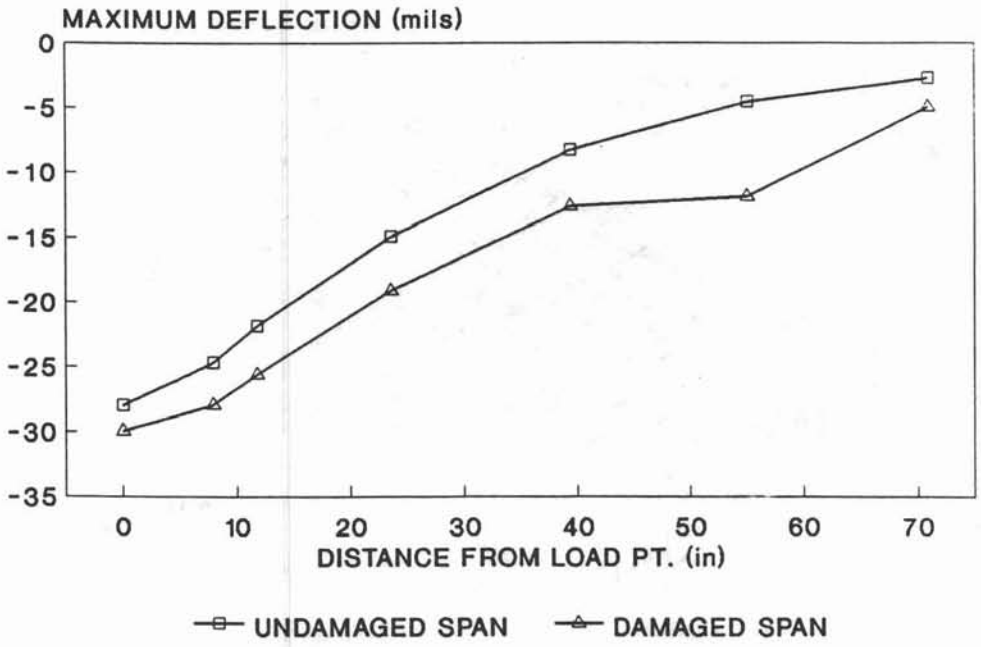

Figure 12
ILM results for damaged and undamaged span drop height = 14.0.

Figure 10 shows the test results for test point 3 with the location of the damage superimposed on the graph. The displacement directly beneath the load was approximately 1.7 times that of test point 1 and 1.6 times that of test point 2. Maximum displacement occurred 8 inches from the load (closer to the damage) instead of directly under the load.

Figures 11 and 12 compare the results of the undamaged and damaged span for the 8.375-inch and 14.0-inch drop heights, respectively. Displacements were greater for the damaged span and the difference is greatest at the point of maximum damage (57 inches from the load point).

Finite Element Analysis

Finite Element Pier Model. NCEL performed a dynamic, linear elastic finite element analysis of the scale model pier using the ADINA finite element code (Refs 20 and 21). A linear elastic analysis was considered adequate since the maximum measured displacements were less than 1/100 of the deck thickness and the undamaged structure responded linearly in the tests. The analysis was simplified by assuming the structural mass could be accurately represented by a lumped mass matrix. The effects of damping were also neglected since damping usually has little effect on the first peak displacement.

The dynamic equilibrium equations were solved in the ADINA program using the Newmark method (Refs 21, 22, and 23). The Newmark method is a direct implicit integration method in which the problem is divided into intervals of time and a step by step numerical

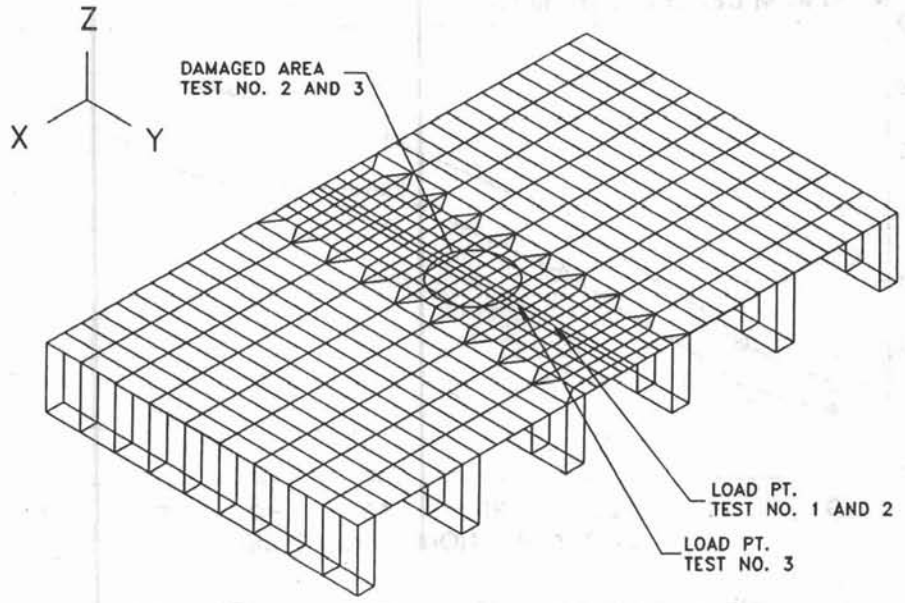

Figure 13
Finite element mesh of NCEL model pier.

integration procedure is performed to solve for the displacements, velocities, and accelerations at each time step.

Figure 13 shows the finite element mesh used in the analysis. The supports were modeled using eight-node, three-dimensional isoparametric elements with 3 degrees of freedom per node. The deck was modeled using four node shell elements with 5 degrees of freedom per node (Refs 20 and 22). Since negligible downward displacements were expected over the supports, the cap beams were modeled using only one element in the vertical direction. The two end deck spans were modeled using a coarse mesh with an element size of 12 inches by 24 inches. The center span was discretized with a refined mesh that included a row of nodes along the center of the span. The typical center span elements were 8 inches by 8.6 inches. The size of the elements along the centerline of the span was 8 inches by 4.3 inches. The transition from the refined mesh to the more coarse mesh was made by using three node shell elements. In addition to the four deck nodes coinciding with the four nodes of a given support element, there are two interior deck nodes that have no corresponding support node. This created the potential for a gap between the deck elements and the support elements. This gap or overlap in the mesh was eliminated by using nodal constraints. Each of the interior nodes was coupled to the adjacent support node. This forced the interior node to undergo the same displacements and rotations as the support node.

Figure 14 shows a section view of the finite element mesh. Since the vertical supports rested continuously on the 2-foot-thick laboratory floor, which prevented downward movement

of the supports, it was assumed that uplift and rotations of the support base could be neglected. Therefore, the bottom nodes were fixed in all degrees of freedom.

Finite Element Model of Impact Load. As noted previously, the impact load function is dependent on the stiffness of the structure. Therefore, Equation 5 cannot be used as the forcing function in the finite element analysis. Instead, the FWD apparatus was modeled as a mass-spring system. This enabled the model to couple the behavior of the FWD to the structure and simulate a more accurate load.

Figure 15 shows the finite element model of the mass-spring concept. The dashed circle shows the area covered by the FWD load plate. The mass of the FWD apparatus was modeled using concentrated nodal masses as shown. Each mass in the figure represents one-sixth of the total drop mass. Each mass node was restrained in all degrees of freedom, except the downward displacement, and given an initial downward velocity determined by Equation 2.

The equivalent spring was represented in the finite element model by truss elements. A truss element has a stiffness defined as follows:

$$K_T = \frac{AE}{L}$$

where A = cross-sectional area of the truss member, $in.^2$

E = modulus of elasticity, ksi

L = member length, inches

The input to the finite element model was simplified by assigning A and L the value of unity so that the stiffness of the truss was represented by a single parameter, E. This parameter was set equal to the equivalent stiffness of the FWD or in this case, E = K/6.

The falling mass was attached to a guide system on the FWD that allowed it to fall freely onto the springs and bounce until it came to rest. After each bounce, the mass actually lost contact with the springs for a period of time. Studies have shown that even for extremely low drop heights, this elapsed time exceeds 180 msec (Ref 24). Since the first peak load occurred in less than 15 msec and the peak displacements occurred within the first 20 msec, the second and subsequent loadings from bouncing were ignored in the finite element analysis just as they were on the FWD. Also, the peak displacements occurred while the mass was still in contact with the springs, therefore, no "gap" or nonlinear truss elements were needed in the analysis. Execution of the analysis was halted before the compression force in the truss members reached zero.

The total drop mass used in the impact load tests was 2.28×10^{-3} kip-sec^2/in. (880 pounds). Each nodal mass represented one sixth of this or 0.38×10^{-3} kip-sec^2/in. The initial downward velocities determined by Equation 2 were 80.45 in./sec for the 8.375-inch drop height and 104.0 in./sec for the 14-inch drop height. The equivalent stiffness of the FWD was determined experimentally for each of the drop heights. (A greater value was used for the 14-

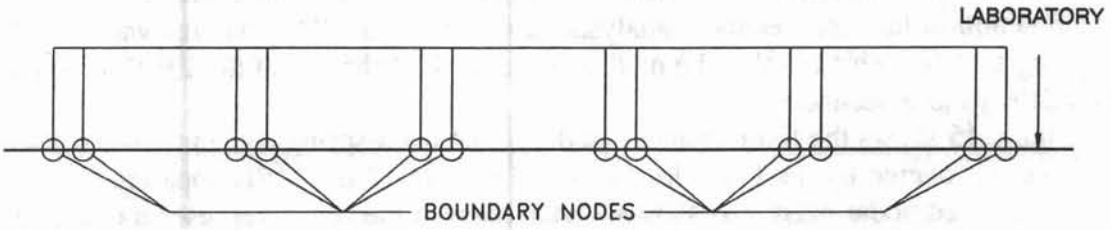

Figure 14
Longitudinal section view of finite element mesh.

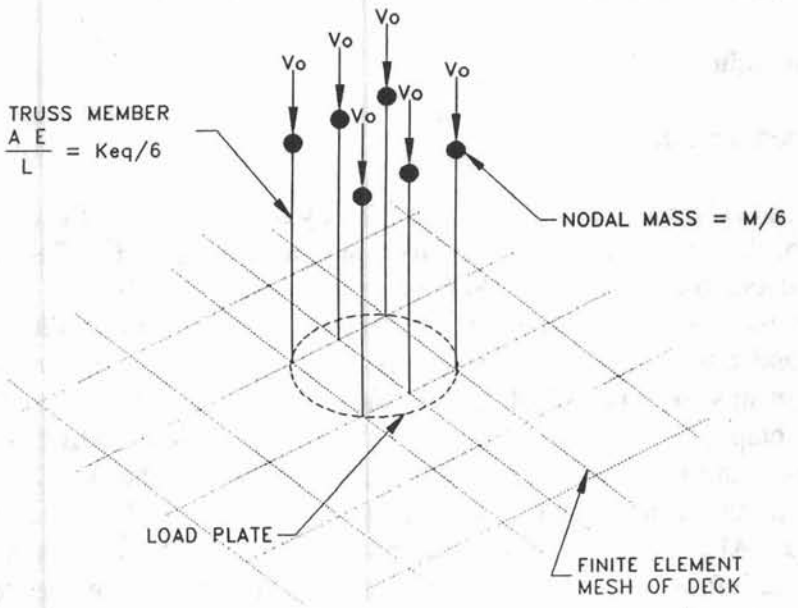

Figure 15
FWD finite element model.

inch drop height to account for the nonlinearity of the elastomeric springs.) The total equivalent stiffnesses were 26.3 kip/in. for the 8.375-inch drop height and 33.6 kip/in. for the 14-inch drop height.

Undamaged Span Modeling and Results. The deflection of a reinforced concrete structure is a function of not only boundary conditions, load, cross section, and material properties but also the amount and extent of flexural cracking. Flexural cracking is dependent upon not only the current load case but the entire load history of the structure. Even with a prior knowledge of the load history of the laboratory structure, it is difficult to determine the effective moment of inertia of the deck. At sections where small bending moments have been applied, the concrete works in both tension and compression. Tensile cracks occur in the concrete at sections of greater moment. These cracks widen and extend to the neutral axis as the moments increase. The tensile stress in the steel between flexural cracks can vary by as much as 60 percent of that across a crack based on the extent of concrete cracking (Ref 25). This further complicates the analysis procedure for predicting the actual deflections. In the case of the pier deck, concrete tensile strength may be even more important since large portions of the deck remain uncracked.

Using the results of the 14-inch drop height for the undamaged span, two models were considered in the finite element analysis. The first model was an isotropic model based on the assumption that the deck was uncracked. The second model was an orthotropic model based on the assumption that the concrete on the tension side of the neutral axis was not effective in resisting the bending forces (cracked).

The isotropic model was based on the gross concrete section ignoring the steel reinforcement. This is a reasonably accurate way of modeling reinforced concrete decks since the effects of the steel reinforcement and the concrete cracking tend to compensate for each other (Ref 26). An elastic modulus of 4,000 ksi and a Poisson's ratio of 0.2 (cylinder test results) were used in the isotropic material model.

The orthotropic model was based on the transformed section properties of the deck in the two principal directions. The stress-strain relationship for the orthotropic material model is as follows (Ref 21):

$$\begin{bmatrix} \sigma_{xx} \\ \sigma_{yy} \\ \sigma_{zz} \\ \tau_{xy} \\ \tau_{xz} \\ \tau_{yz} \end{bmatrix} = \begin{bmatrix} E_{xx} & E_{xy} & 0 & 0 & 0 & 0 \\ E_{xy} & E_{yy} & 0 & 0 & 0 & 0 \\ 0 & 0 & 0 & 0 & 0 & 0 \\ 0 & 0 & 0 & G_{xy} & 0 & 0 \\ 0 & 0 & 0 & 0 & G_t & 0 \\ 0 & 0 & 0 & 0 & 0 & G_t \end{bmatrix} \begin{bmatrix} e_{xx} \\ e_{yy} \\ e_{zz} \\ \gamma_{xy} \\ \gamma_{xz} \\ \gamma_{yz} \end{bmatrix} \quad (7)$$

where x and y represent the principal orthogonal directions and z represents the direction through the thickness of the element.

In order to use this model, the five material constants E_{xx}, E_{yy}, E_{xy}, G_{xy}, and G_t are required. These values are based on the transformed section properties in each direction and are defined as follows (Ref 27):

$$E_{xx} = \frac{12}{h^3} \frac{E_c}{1-\mu^2} \left[I_{cx} + (n-1)\, I_{sx_c} + n\, I_{sx_t} \right] \tag{8}$$

$$E_{yy} = \frac{12}{h^3} \frac{E_c}{1-\mu^2} \left[I_{cy} + (n-1)\, I_{sy_c} + n\, I_{sy_t} \right] \tag{9}$$

$$E_{xy} = \mu\sqrt{E_{xx}\, E_{yy}} \tag{10}$$

$$G_{xy} = \frac{1-\mu}{2} \sqrt{E_{xx}\, E_{yy}} \tag{11}$$

$$G_t = \frac{E_c}{2(1+\mu)} \tag{12}$$

where E_c = elastic modulus of concrete, ksi

μ = Poisson's ratio of concrete

h = thickness of slab, inches

n = E_s/E_c

E_s = elastic modulus of steel, ksi

I_{cx}, I_{cy} = effective concrete moment of inertia about the neutral axis for sections x and y, respectively.

I_{sx_c}, I_{sy_c} = moment of inertia of the compression steel about the neutral axis for sections x and y, respectively.

I_{sx_t}, I_{sy_t} = moment of inertia of the tension steel about the neutral axis for sections x and y, respectively.

In determining the moment of inertia values required in Equations 8 through 12, the elastic constants were calculated for each of the three sections (middle span, near support, and over support) shown in Figure 5 using E_c equal to 4,000 ksi and μ equal to 0.2. The values of the elastic constants for each section are listed in Table 2 (see Figure 13 for x and y orientation).

Table 2
Elastic Constants for Initial Orthotropic Pier Model (ksi)

Section	E_{xx}	E_{yy}	E_{xy}	G_{xy}	G_t
A	1,300	199.1	762.4	398.3	1,679
B	1,103	156.3	558.6	312.5	1,679
C	1,300	260.0	1,300.0	520.0	1,679

For a given time step, the force imparted to the structure by the mass-spring model can be determined by summing the compressive forces in the six truss members shown in Figure 15. Figure 16 is a plot of this sum for both drop heights for the time period between 0 and 20 msec. The peak load occurred at 14 msec for the 8.375-inch drop height and at 13 msec for the 14-inch drop height. The maximum deflections of the deck occurred at 16 msec or less. Therefore, all finite element runs were halted at 20 msec. The calculated loads were similar to the sine load given in Equation 5. The peak load for the 8.375-inch drop height from Figure 16 was 19.9 kips. The measured load for this drop height averaged 19.7 kips (Table 1). The peak load for the 14-inch drop height was 28.3 kips and the measured load for this drop height averaged 28.1 kips. The finite element results were within 1 percent of the measured loads.

Figure 17 compares the deflections for the isotropic finite element model, the orthotropic finite element model, and the impact load test for the 14-inch drop height. The measured behavior was halfway between the isotropic and orthotropic models in the region directly beneath the load. The orthotropic results were closer to the measured deflections in the region away from the load.

Since the ILM results more closely matched the orthotropic model, it was used for the remainder of the finite element analysis. This model was calibrated by increasing the moment of inertia terms, E_{xx}, E_{yy} in Equations 8 and 9 until the finite element results best matched the measured displacements. This increase was made uniformly throughout the deck in both directions. Figures 18 and 19 compare the results of the calibrated orthotropic model with the ILM results for the 8.375-inch and 14.0-inch drop heights, respectively, where moment of inertia terms E_{xx} and E_{yy} are increased by 47 percent over those of Table 2. The figures show close agreement between the calculated and measured results. The averages of the measured displacements directly beneath the load were 19.7 and 28.0 for the 8.375- and 14.0-inch drop heights, respectively. The finite element results were 20.3 and 28.4. The finite element results away from the load were even closer to the measured values.

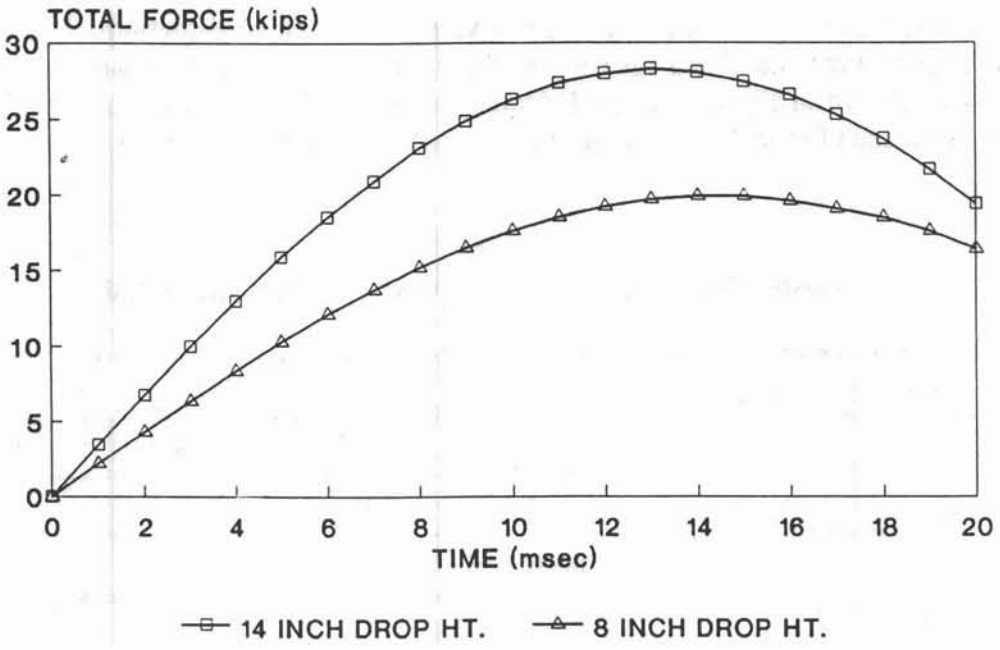

Figure 16
Finite element results of load for test point 1.

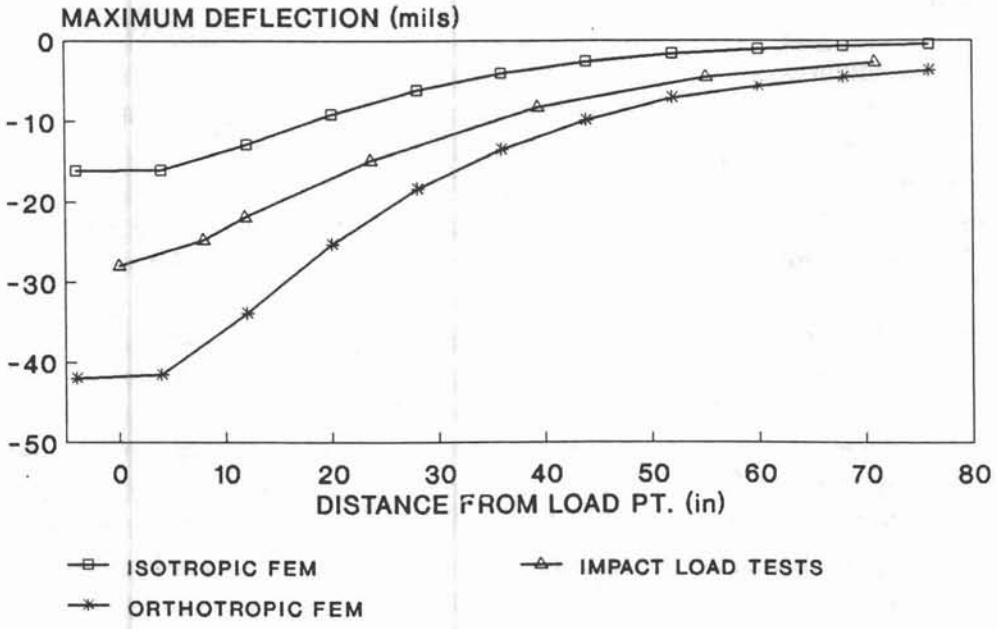

Figure 17
Uncalibrated finite element results for test point 1, 14-inch drop height.

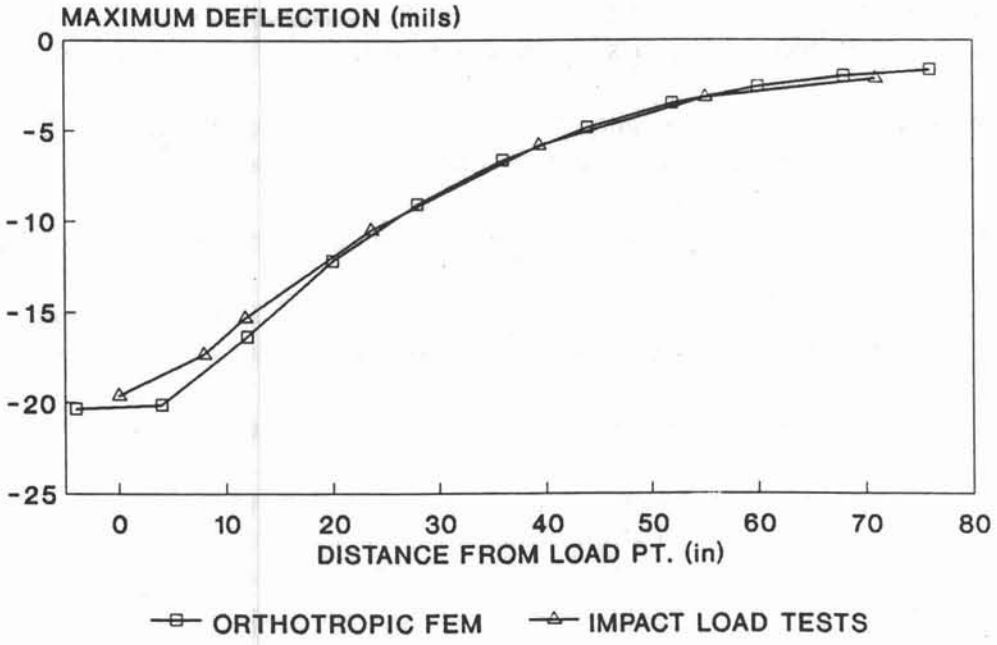

Figure 18
Finite element results for test point 1, 8.375-inch drop height.

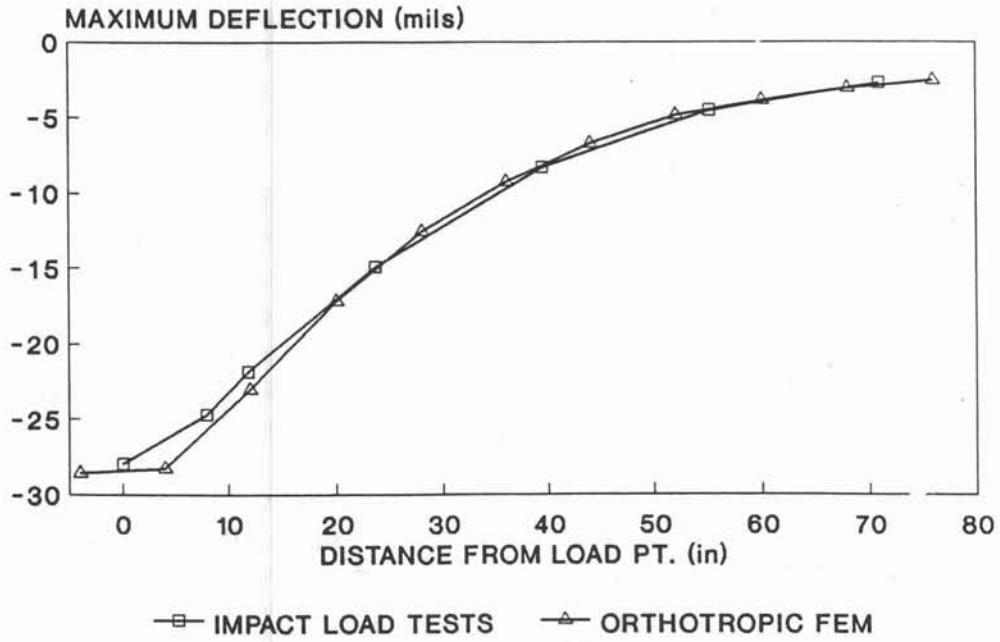

Figure 19
Finite element results for test point 1, 14-inch drop height.

Damaged Modeling and Results. The internal condition of the model pier deck in the damaged area was unknown. However, based on the crack patterns, type of loading, and observed shear failure, the following assumptions were made based on surface observations and measured load-deflection characteristics (these assumptions are illustrated in Figure 20a):

- Diagonal cracks wide enough to preclude aggregate interlock propagated from the perimeter of the load through the thickness of the deck.
- Extensive cracking occurred in the cone of concrete below the diagonal cracks.
- Complete loss of bond between the concrete and the reinforcing steel occurred for the bottom layer of reinforcement within the area of visible damage.
- Flexural cracks occurred in the concrete above the diagonal cracks.

The damage above was represented in the finite element model by a reduction in the effective moment of inertia of the deck (from that of the undamaged deck model). The portion of the deck contributing to the stiffness was assumed to be similar to that shown in Figure 20b in calculating this effective moment of inertia. The bottom layer of reinforcing steel and a large portion of the concrete below the top layer of steel was ignored in computing the moment of inertia of the damaged section. Figure 21 shows a plan view of the finite element mesh of the damaged span. The dashed circle represents the approximate area of visible damage. The elastic constants defined in Equations 8 through 11 were computed for the elements in the shaded area based on the reduced section of Figure 20b. The elastic constant G_t defined by Equation 12 was reduced by the ratio h^3_{eff}/h^3 where h_{eff} is the effective thickness of the slab shown in Figure 20b and h is the actual slab thickness. This had the effect of smearing the equivalent stiffness over the thickness of the original element. By modeling the damage in this way, the stiffness was reduced (h^3_{eff}/h^3 = 0.67 percent of that of the undamaged section) while the thickness of the deck along with its mass remained the same. The reduced stiffness was assumed to be constant for the shaded elements in Figure 21.

Figure 22 compares the results of the initial, damaged finite element model of constant damage with the measured test results for the 8.375-inch drop height of test point 2. The finite element results did compare favorably for the region directly under the load but the displaced shape suggested that a further refinement to the model was needed.

In the initial case, it was assumed that the zone in which the flexural cracks existed did not contribute to the flexure and shear stiffness in the damaged area (see Figures 20a and 20b). To refine the damaged model, it was assumed that aggregate interlocking enabled the deck to transmit shear forces across these flexural cracks. Therefore, the concrete considered to be effective in transmitting shear was assumed to vary linearly as shown in Figure 20c. This changed the way in which the load was distributed in the slab. The values of G_t for each row of elements were computed based on the average effective thickness across the element (varying from full value to 0.1 percent of the undamaged section). The remaining elastic constants were not changed from the initial damaged model.

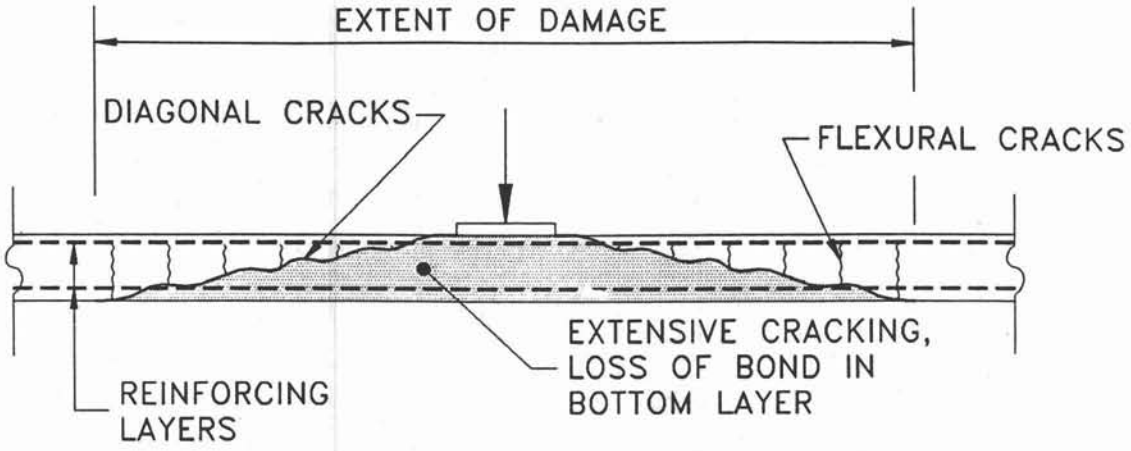

(a) Actual structure.

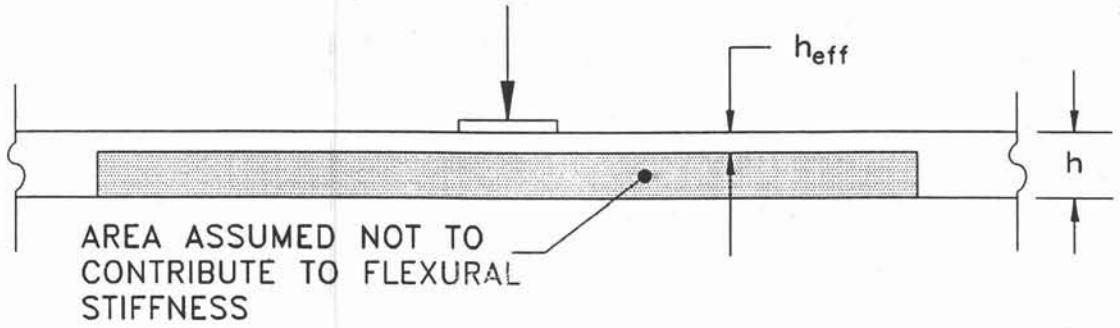

(b) Constant effective thickness.

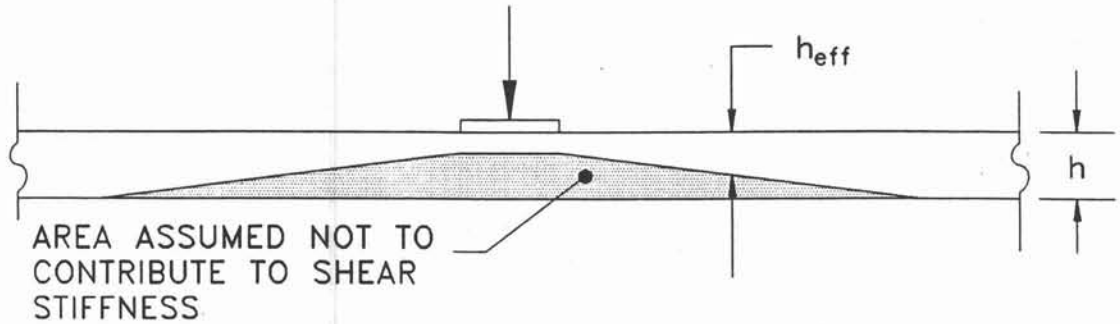

(c) Linearly varying effective thickness.

Figure 20
Characteristics of damaged span.

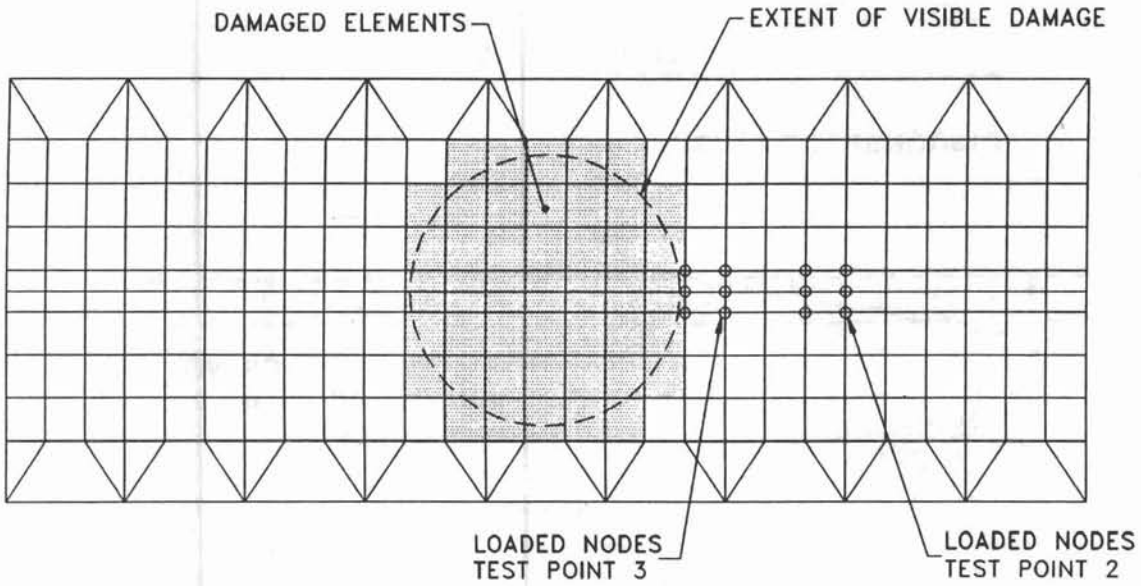

Figure 21
Plan view - finite element mesh of damaged span.

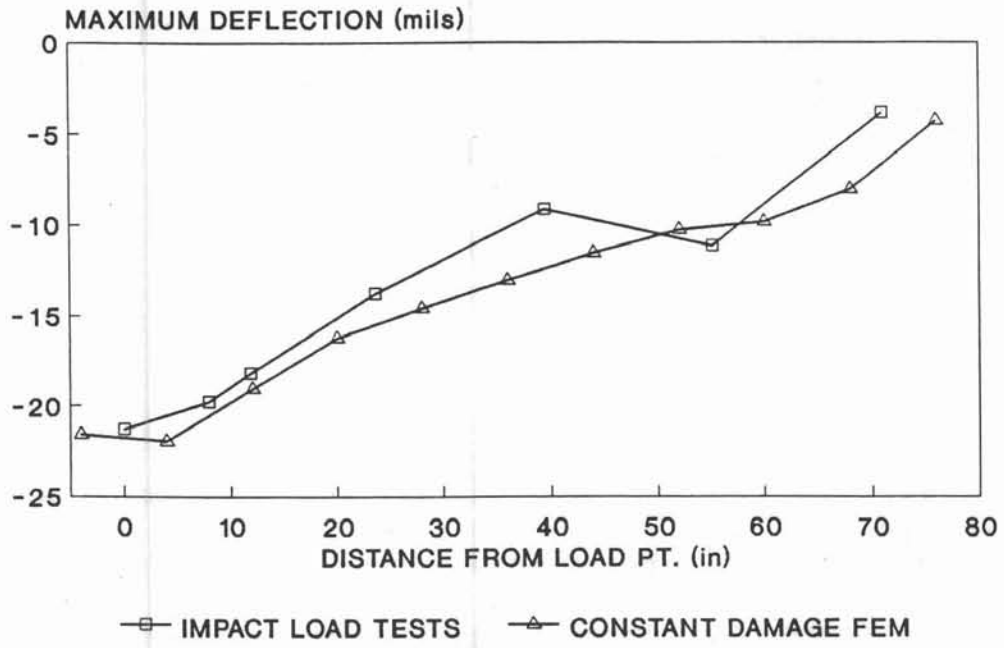

Figure 22
Finite element results of constant damage model test point 2, 8.375-inch drop height.

Figure 23 compares the results of the more refined finite element model for the damaged span with the ILM test results. The finite element results of the undamaged span are also shown. This model agreed much closer with the test results. Not only did the calculated deflections match the measured values under the load, but the characteristic change in slope at the damaged area matched as well. Because of its close agreement, the refined model was used to represent the damaged span for sensitivity studies.

Damaged Finite Element Model Results. The finite element model of the FWD on the damage span model matched the measured loads for test point 2. The maximum loads determined by the finite element model were 19.9 and 28.3 kips for the 8.375- and 14.0-inch drop heights, respectively. The measured values were 19.6 and 28.6. The calculated loads for test point 3 were not as close to the measured results. The finite element model yielded loads of 19.7 and 28.0 for the 8.375- and 14.0-inch drop height, respectively. The measured values were 21.0 and 29.4.

Figure 24 compares the results of the ILM tests and the finite element analysis for the 14-inch drop height at test point 2. For reference, the finite element results of the undamaged span are also shown. Close agreement existed between the calculated values and the measured results for the region directly beneath the load. However, unlike the 8.375-inch drop height, the finite element model did not accurately model the region close to the damage.

Figures 25 and 26 compare the results of the ILM tests and the finite element analysis at test point 3 for the 8.375-inch and 14.0-inch drop heights, respectively. The calculated values for the displacements differed slightly from the measured results; however, the overall shape of the plots compared favorably.

Damage Sensitivity Analysis of the Deck

The method of modeling the damaged areas discussed in the previous section was used to conduct a damage sensitivity analysis of the deck. The two parameters investigated were the size of the damaged area and the distance from the impact load point to the center of the damage. The parameters within the damaged area were not changed from those of the more refined model described in the previous section. Figure 27 shows a plan view of the center span finite element mesh. The load point (point A) was located at the center of the span, and the center of the damaged elements (point B) was located a distance, x, from the load point. Four damaged areas corresponding to 23, 12, 4.3, and 0.5 ft^2 on the actual structure were considered. Each damaged area was rectangular as shown in the figure. The load point was at the center location for all cases and the values used for x were 0, 40, and 80 inches. Each of the nodal masses in the FWD model were given an initial velocity corresponding to the 14-inch drop height.

Table 3 contains the results of the sensitivity analysis. Maximum displacements were calculated at the load point (point A) and at the center of the damage (point B) for each of the damaged area and distance combinations. The ratio of the displacements for the damaged to undamaged results for points A and B are also given in the table.

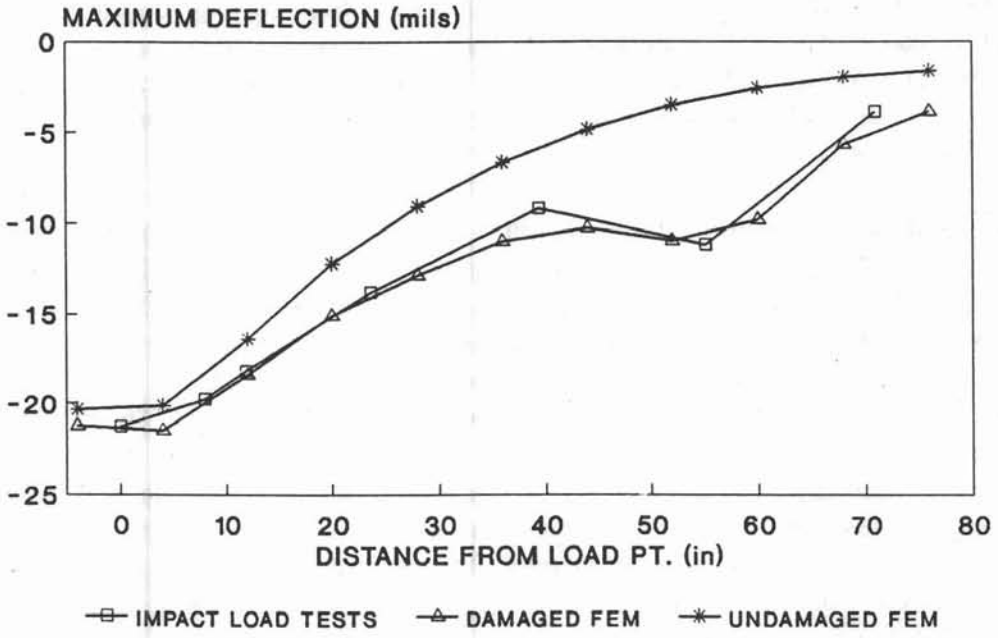

Figure 23
Finite element results for test point 2, 8.375-inch drop height.

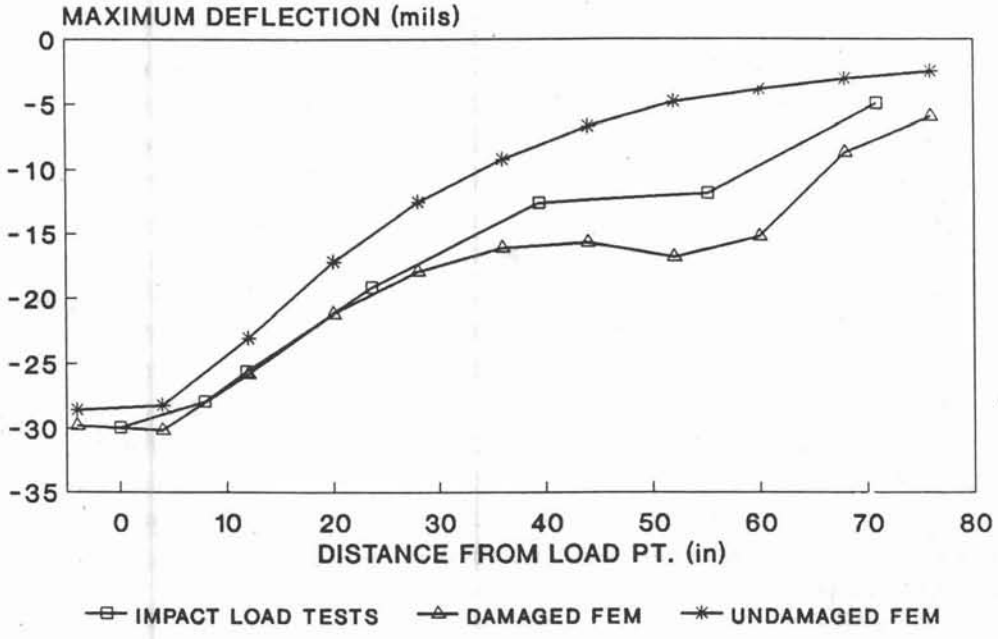

Figure 24
Finite element results for test point 2, 14-inch drop height.

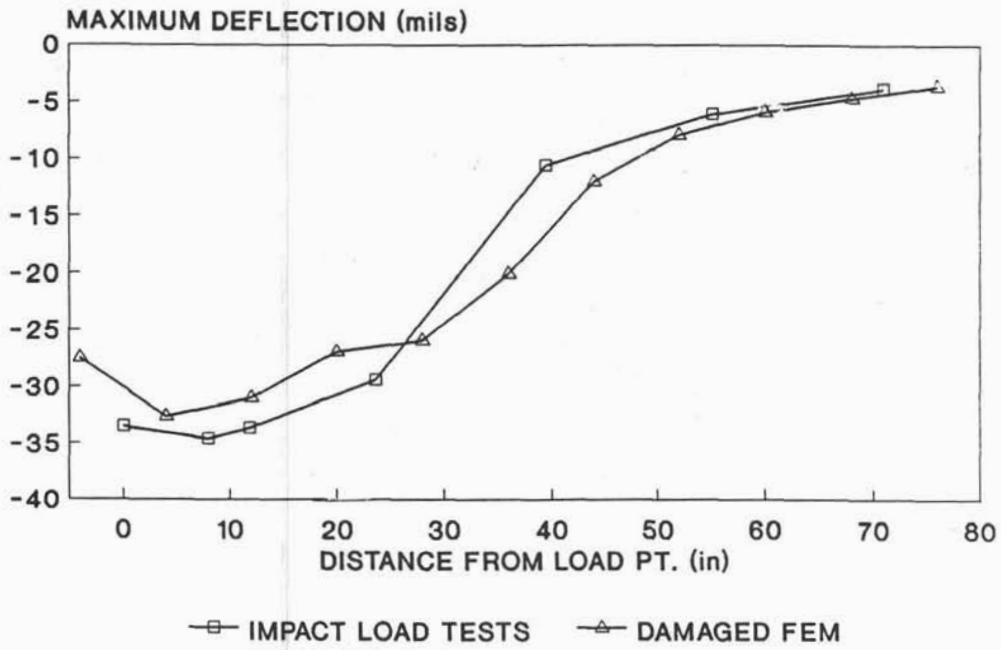

Figure 25
Finite element results for test point 3, 8.375-inch drop height.

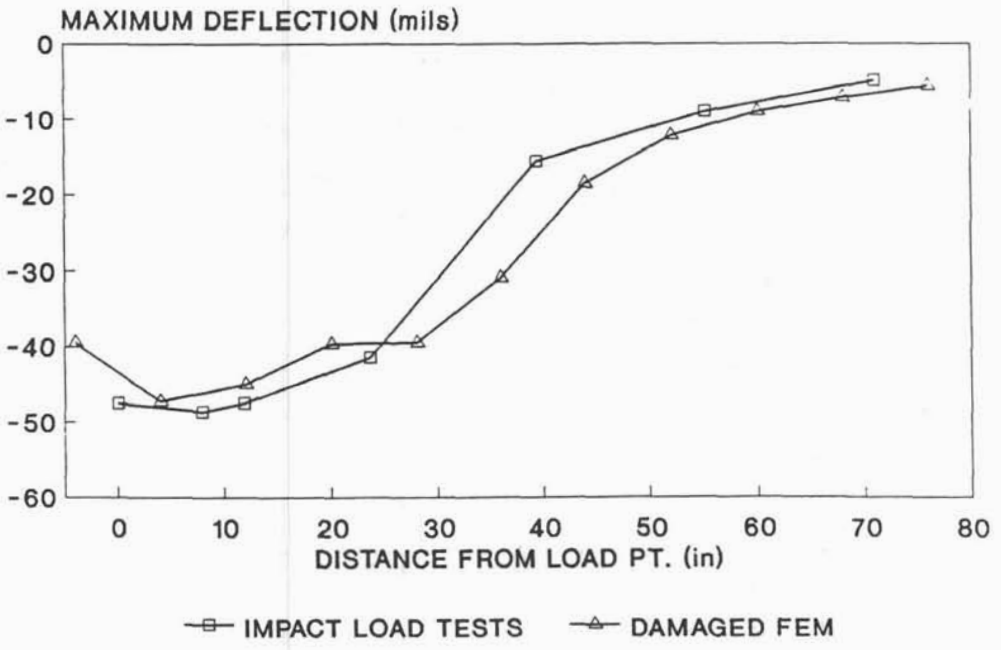

Figure 26
Finite element results for test point 3, 14-inch drop height.

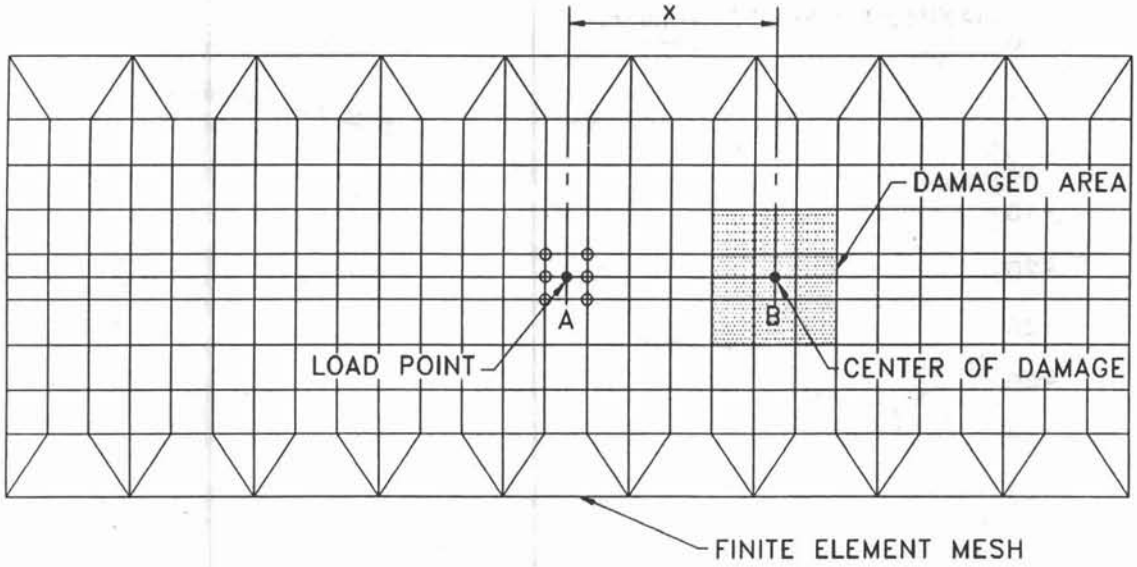

Figure 27
Plan view - finite element mesh of center span showing sensitivity parameters.

Table 3
Results of Deck Sensitivity Analysis

Damaged Area (ft^2)	x (in.)	Damaged Span Displacements (mils)		Ratio of Displacements Damaged/Undamaged	
		Pt. A	Pt. B	Pt. A	Pt. B
23	0	220	220	7.8	7.8
23	40	37	32	1.3	4.1
23	80	28	10	1.0	3.4
12	0	110	110	4.0	4.0
12	40	29	15	1.1	1.9
12	80	28	5.1	1.0	1.7
4.3	0	85	85	3.1	3.1
4.3	40	28	11	1.0	1.4
4.3	80	28	3.8	1.0	1.3
0.5	0	31	31	1.1	1.1
0.5	40	29	8.3	1.0	1.1
0.5	80	28	3.1	1.0	1.0

An increase in displacement occurred at point A in all cases where the load point was located directly over the damage (x = 0). As x increased, the displacements at point A approached those of the undamaged span. The damaged area had no influence on the displacement under the load in the cases where x was equal to 80 inches. An increase in displacements at point B was observed in all cases except where the area was 0.5 ft^2 and x was equal to 80 inches. Figure 28 shows how the ratio of the damaged to undamaged displacements at point B changes as the distance, x, increases.

Although the finite element results showed that displacements for the damaged span were greater than those of the undamaged span, there were resolution problems in cases where the displacements were small. For example, the displacement in the undamaged span was approximately 3 mils at 80 inches from the load point. In the case where the damaged area was 4.3 ft^2, the displacement increased by a factor of 1.3 to 3.8 mils. The ability of the FWD measuring system to accurately resolve such small displacements is questionable. However, the finite element results did indicate that small to moderately sized damaged areas can be detected provided the impact load points are positioned near enough to the damaged area.

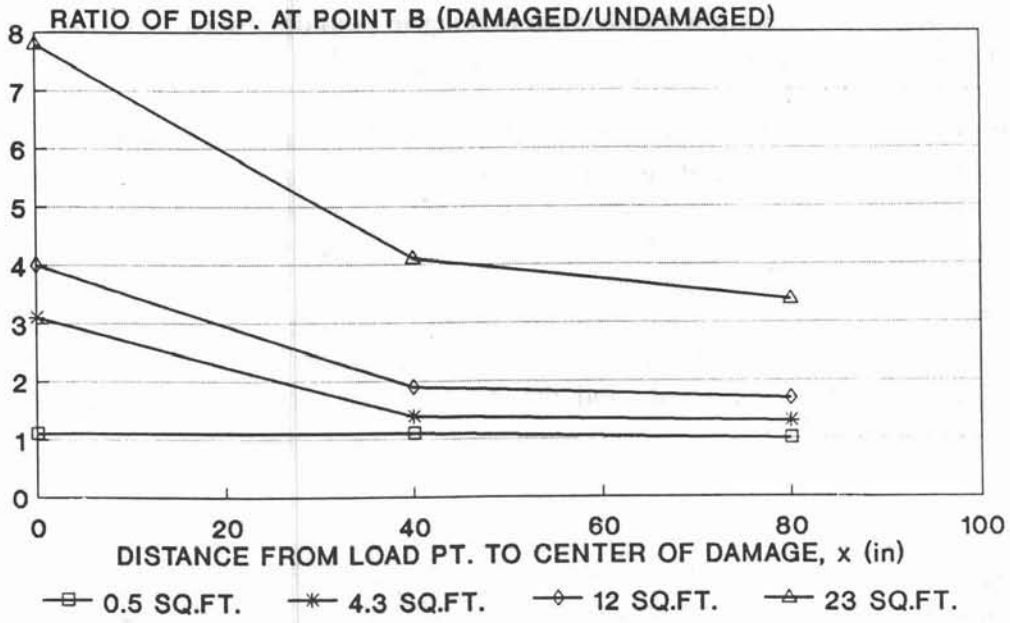

Figure 28
Ratio of damaged to undamaged finite element results at center of damage (point B).

HIGHWAY BRIDGE TESTS

Description

The highway bridge, HB-4, is located over the Swimming River at Naval Weapons Station (WPNSTA), Earle, New Jersey. The bridge is part of the Normandy Road system used to transport weapons and munitions from storage magazines to pierside. HB-4 was built in 1944 and has been used extensively in support of Atlantic Fleet operations (Ref 28). WPNSTA Earle provided logistic support and technical review of the tests in return for load assessment of the bridge.

Geometry. HB-4 is 432 feet long with a roadway width of 20 feet (Figures 29 and 30). The structure consists of a 12-inch-thick concrete deck reinforced with No. 7 bars and supported by timber pile bents spaced at 12 feet. The deck has an asphalt overlay of 1 to 3 inches and is continuous over the pile bents except for four expansion joints located 96 feet apart. Beams approximately 4 feet deep and 1.5 feet wide at the base and tapering to 0.5 foot at the top are located on each side of the deck. These beams, which were cast monolithically with the deck, serve as guard rails and contribute to the flexural stiffness of the superstructure.

The structure has 37 pile bents designated alphabetically from A at the north end to KK at the south end. A typical pile bent consists of a 12-inch by 12-inch timber cap supported by four, 12-inch-diameter timber piles with cross bracing in both directions. The two interior piles are vertical and the two exterior piles are battered 1.5 to 12.

Condition. A general inspection of HB-4 in 1990 revealed external rot and scouring of several piles, damaged and missing secondary members, and chemical attack on bolted connections (Ref 28). Concrete cracking and spalling were observed in the deck, particularly in the vicinity of the expansion joints. Gaps as large as 1 inch were observed between the pile and the pilecap at four different locations.

During early 1991, before the ILM tests were conducted, maintenance was performed on the bridge to correct some of the deficiencies. The expansion joints were rebuilt, dips in the roadway were leveled with asphalt, and the gaps between the pilecaps and the piles were shimmed.

ILM Tests

Setup. NCEL performed ILM tests on a 192-foot section of the bridge from pile bent F to pile bent V inclusively. The entire test series required less than one-half day. The load points were located near the center line and the displacement sensors were oriented perpendicular to the flow of traffic. The load points had to be offset from the center line 1 foot so that the FWD trailer could clear the bridge side beams (guard rails). Figure 31 shows the location of the load point and the orientation of the sensors for a typical pile bent and midspan test. Tests were performed at each pile bent and at the middle of each span. Two passes were made in order to record the response of both the east and west sides. The load points were shifted at the expansion joints located at pile bents F, N, and V to either side of the joint to avoid spanning the joint opening. The test points were located 6 inches (one-half of the diameter of the load plate) south on pile bent F and 6 inches north on pile bent V. Pile bent N was tested on each side of the expansion joint.

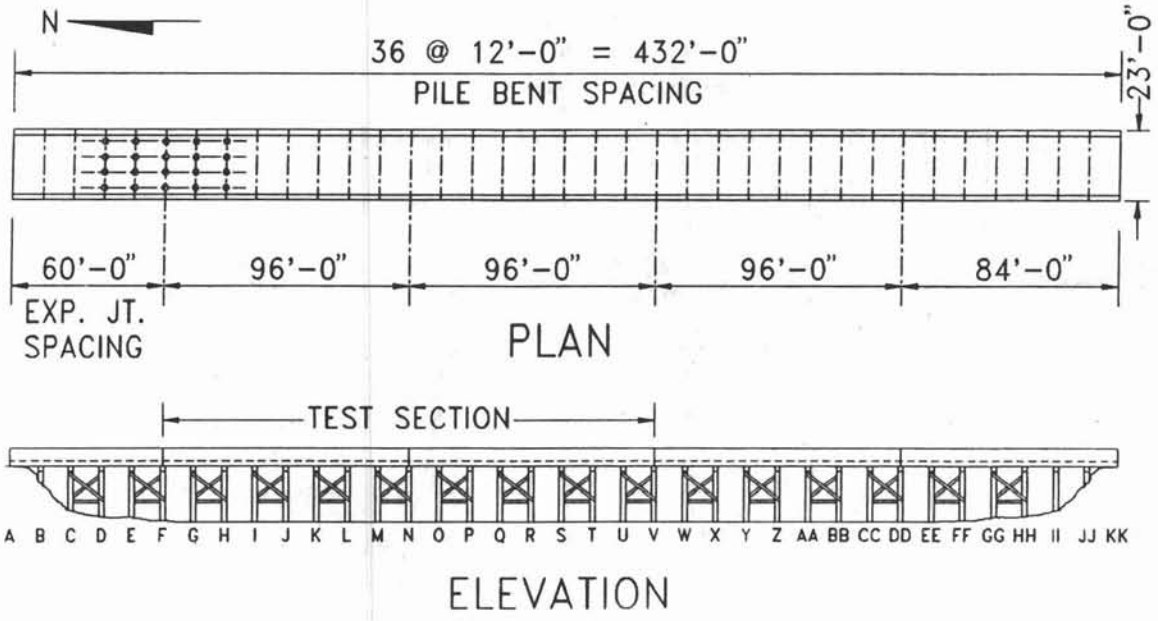

Figure 29
Plan and elevation views of HB-4.

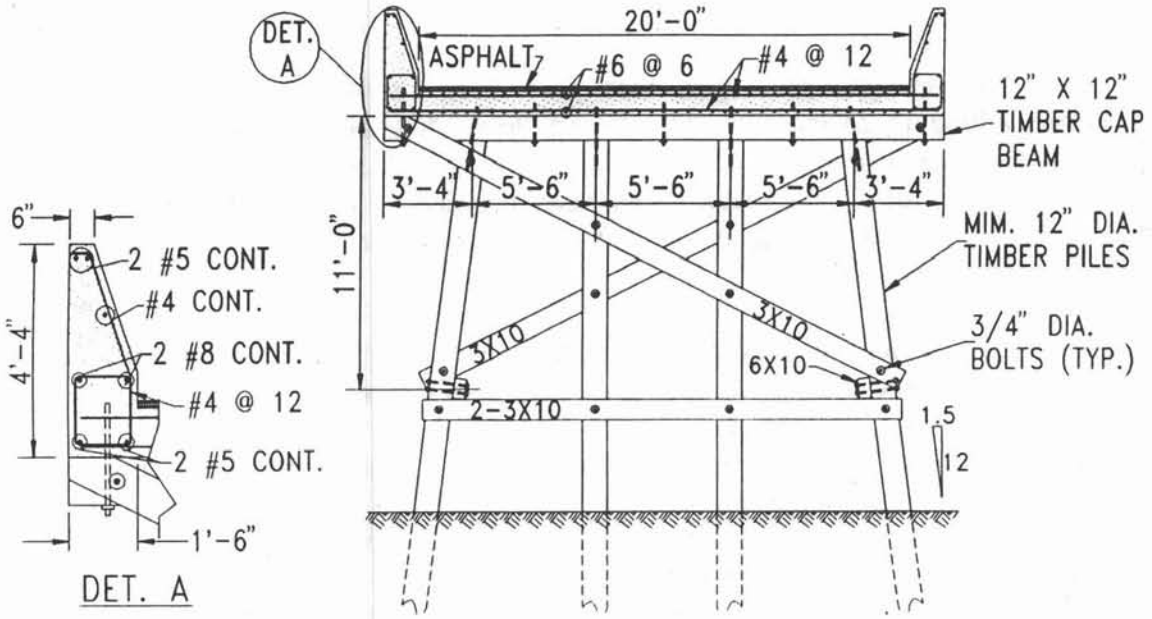

Figure 30
Section view of HB-4.

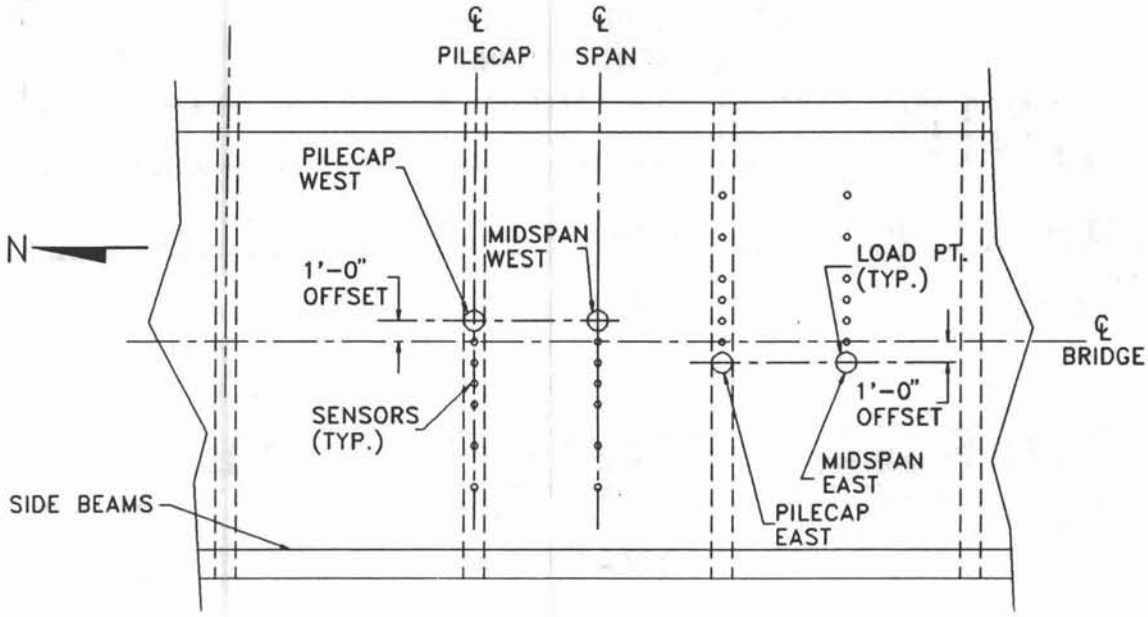

Figure 31
Plan view showing test point locations and sensor locations.

Three tests were performed at each test point using a constant mass drop combination of 1,540 pounds falling 15.25 inches. The goal was to produce peak loads of approximately 50 kips. The FWD system processor was programmed to record the entire load and displacement histories of the three tests. The history files were recorded using ASCII format on 3-1/2-inch floppy diskettes. In addition, a hard copy of the peak loads and maximum displacements was printed as the tests were being conducted.

Results. The three tests performed at each test point produced essentially equivalent results for both loads and displacements. To simplify the following discussion, the results of a single test were used for each test point.

The peak loads and maximum displacements for each test point are given in Tables 4 through 7. The peak loads ranged from 47.76 kips at span U-V - West to 51.86 kips at pilecap R - East. The average peak load for both sides was 50 kips, and the variation was due to the relative stiffness of the bridge at the load point.

Figure 32 shows the load histories for a typical pile bent and midspan test. The load resembled a half sine wave with a duration of approximately 35 msec. A dip in the load curve was observed at approximately 12 msec for all test points. This can be attributed to the multi-degree-of-freedom nature on the FWD apparatus coupled to the bridge structure.

Table 4
ILM Test Results - Pile Bent - East Side

Test Pt.	Peak Load (kips)	Maximum Deflection (mils) for Sensor Location (in.)						
		0	12	24	36	48	72	96
F2	49.68	61.01	52.54	48.74	44.45	39.96	30.37	22.52
G	50.61	46.48	38.73	35.69	33.20	30.18	22.63	15.31
H	49.85	54.08	43.09	39.77	36.34	32.56	23.94	16.15
I	50.32	53.91	45.74	43.44	40.61	37.31	28.65	19.99
J	50.61	44.98	40.75	39.05	35.91	30.64	23.96	17.06
K	50.79	45.26	43.83	40.49	37.38	34.25	26.18	18.07
L	50.12	49.48	45.86	43.52	40.84	37.58	28.96	20.47
M	51.15	45.17	42.51	39.71	36.86	33.69	26.03	18.32
N1	49.97	57.30	54.91	50.40	46.04	41.07	30.90	21.68
N2	50.11	55.29	55.04	51.79	47.91	43.98	34.13	23.95
O	52.00	43.88	42.28	40.34	38.20	35.24	27.31	19.38
P	51.68	42.72	37.43	34.93	32.31	29.47	22.18	15.66
Q	51.85	42.28	40.13	38.50	36.67	34.18	27.15	19.73
R	51.86	37.95	35.54	32.93	31.95	29.51	23.45	13.84
S	50.46	51.86	48.92	45.72	43.21	39.80	31.72	23.25
T	51.18	42.01	39.94	37.46	35.89	33.29	26.19	18.73
U	51.30	46.43	45.51	42.83	40.72	37.94	30.43	21.95
V1	49.74	54.02	52.31	47.80	44.33	40.24	30.53	21.49

Table 5
ILM Test Results - Pile Bent - West Side

Test Pt.	Peak Load (kips)	Maximum Deflection (mils) for Sensor Location (in.)						
		0	12	24	36	48	72	96
F2	50.49	56.07	53.30	49.51	44.79	40.19	30.60	22.35
G	50.27	44.08	38.39	35.85	33.43	30.61	23.36	16.09
H	49.71	53.99	41.69	38.99	36.17	33.12	25.03	17.91
I	50.11	53.23	46.05	43.06	39.37	35.77	26.92	18.71
J	49.91	43.40	40.96	38.49	35.43	32.83	25.41	17.80
K	49.35	45.08	42.73	40.43	38.28	36.00	28.39	19.97
L	49.14	53.48	47.31	.65	40.25	36.94	28.61	19.81
M	49.70	44.88	43.25	40.75	38.30	35.13	26.82	18.29
N1	48.67	55.04	53.80	49.10	44.32	39.74	29.86	20.21
N2	49.41	57.29	56.16	52.33	47.94	43.10	32.21	21.68
O	48.91	53.32	42.92	39.93	37.02	34.13	26.07	17.91
P	49.10	43.56	37.59	34.97	32.07	29.28	22.16	15.73
Q	48.83	45.59	42.02	38.93	35.53	32.69	24.28	16.20
R	50.99	40.81	36.71	34.03	31.39	28.41	21.26	14.49
S	50.83	48.57	48.43	46.65	44.25	41.01	31.84	22.60
T	49.57	44.45	40.69	37.71	35.08	32.34	25.00	17.34
U	48.45	63.63	46.20	42.15	38.59	34.96	26.18	18.36
V1	48.92	55.33	51.58	47.52	43.48	39.26	29.44	20.33

Table 6
ILM Test Results - Midspan - East Side

Test Pt.	Peak Load (kips)	Maximum Deflection (mils) for Sensor Location (in.)						
		0	12	24	36	48	72	96
F-G	51.18	54.10	50.69	48.00	44.85	40.82	31.34	21.90
G-H	49.71	65.24	52.91	48.89	44.56	40.21	29.37	19.57
H-I	49.59	64.81	56.39	53.24	49.79	45.11	33.52	22.55
I-J	50.63	61.54	53.61	50.61	46.88	43.04	32.76	22.49
J-K	51.50	57.52	51.78	48.67	45.34	41.64	31.83	22.25
K-L	49.78	63.73	58.74	55.21	51.05	46.73	35.28	24.11
L-M	50.81	60.04	55.11	51.83	48.36	44.32	33.85	23.63
M-N	50.38	60.81	57.06	53.99	50.10	45.71	34.39	23.74
N-O	50.82	55.22	57.12	53.48	50.24	46.26	36.11	24.83
O-P	50.61	58.04	49.40	47.06	43.68	40.39	30.89	21.21
P-Q	51.61	42.06	40.35	38.48	36.58	34.19	27.10	19.74
Q-R	50.88	49.49	47.07	44.97	42.48	39.44	30.94	22.16
R-S	50.45	49.17	46.22	43.95	41.96	39.22	30.70	22.03
S-T	50.20	52.35	48.54	45.43	43.18	39.94	31.22	22.37
T-U	51.47	53.34	54.72	47.99	46.52	42.98	32.65	23.34
U-V	49.80	55.43	56.18	53.04	49.64	45.54	34.58	23.70

Table 7
ILM Test Results - Midspan - West Side

Test Pt.	Peak Load (kips)	Maximum Deflection (mils) for Sensor Location (in.)						
		0	12	24	36	48	72	96
F-G	50.68	54.61	50.25	47.47	44.70	41.33	31.89	22.37
G-H	49.86	55.86	51.22	48.46	45.09	41.43	31.16	21.45
H-I	49.16	66.12	56.44	52.97	48.98	44.09	33.02	21.91
I-J	49.49	57.39	53.18	50.48	47.29	43.54	33.20	22.68
J-K	49.65	53.96	50.72	48.49	46.00	42.78	32.85	22.42
K-L	49.43	63.30	56.68	54.49	51.91	48.65	38.74	27.57
L-M	48.27	61.96	54.28	51.69	48.36	44.29	33.88	23.48
M-N	48.74	63.76	58.23	54.48	50.04	45.35	33.98	22.95
N-O	49.08	58.52	56.93	52.13	47.77	43.16	32.05	19.74
O-P	48.57	57.89	48.84	45.84	43.04	39.12	30.39	21.26
P-Q	49.50	66.26	57.30	53.24	49.01	44.39	33.08	22.10
Q-R	48.53	55.03	47.81	44.87	41.78	37.93	28.72	19.54
R-S	50.90	50.00	47.59	44.87	42.09	38.44	29.33	20.08
S-T	50.17	50.96	48.32	46.31	43.80	40.47	31.45	22.47
T-U	47.95	67.23	53.85	49.78	45.50	41.22	30.59	21.21
U-V	47.76	79.10	58.46	53.80	49.02	44.34	32.69	21.67

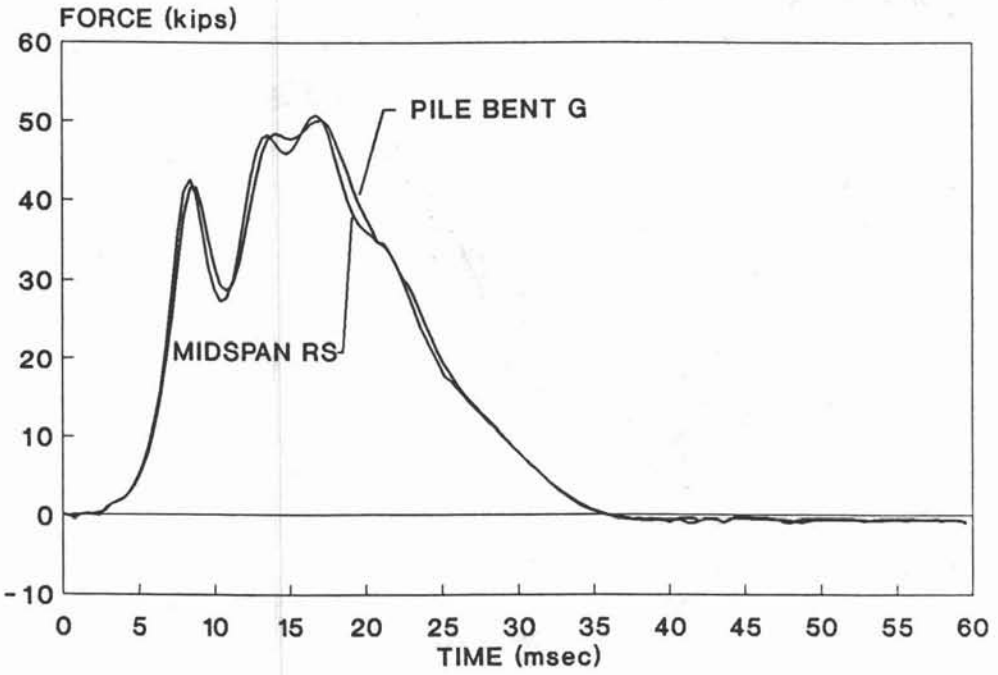

Figure 32
ILM load histories for typical pile bent and midspan tests.

Figures 33 and 34 show displacement histories of each of the seven sensors for a typical pile bent and midspan test. By integrating velocities to obtain displacements, the fluctuations typically observed in experimental data are eliminated. Therefore, each graph shows a set of smooth sinusoids. The maximum displacements occurred at 20 to 25 msec for each of the tests. The load reached zero at about 35 msec and the structure underwent a free vibration phase where the maximum upward displacements were usually less than one-third of the downward displacements.

The results of individual tests were examined following a similar approach used on the pier model. The maximum deflections at each sensor were used to define a characteristic deflected shape of the bridge deck for each test point. These deflected shapes were then plotted and used to determine the correlation between ILM results and visual inspections.

The visual inspection found pile bents P and G to be in excellent condition and the best condition for HB-4. This was reflected in the ILM results where displacement patterns were distributed similar to classic plate response. Figure 35 shows the deflection basin plots (maximum sensor response) for these two locations. Pile bents P and G were among those that experienced the smallest displacements. The maximum deflections occurring at the load point were in the 40- to 50-mil range. The deflection basins have a constant slope except for the area directly under the load. This excess deflection under the load is attributed to compressing the asphalt pavement to magnify the displacement measurements at the load point. There was no asphalt effect on the sensor measurements away from the load point. The asphalt in this area simply moved with the surface of the concrete deck without deforming.

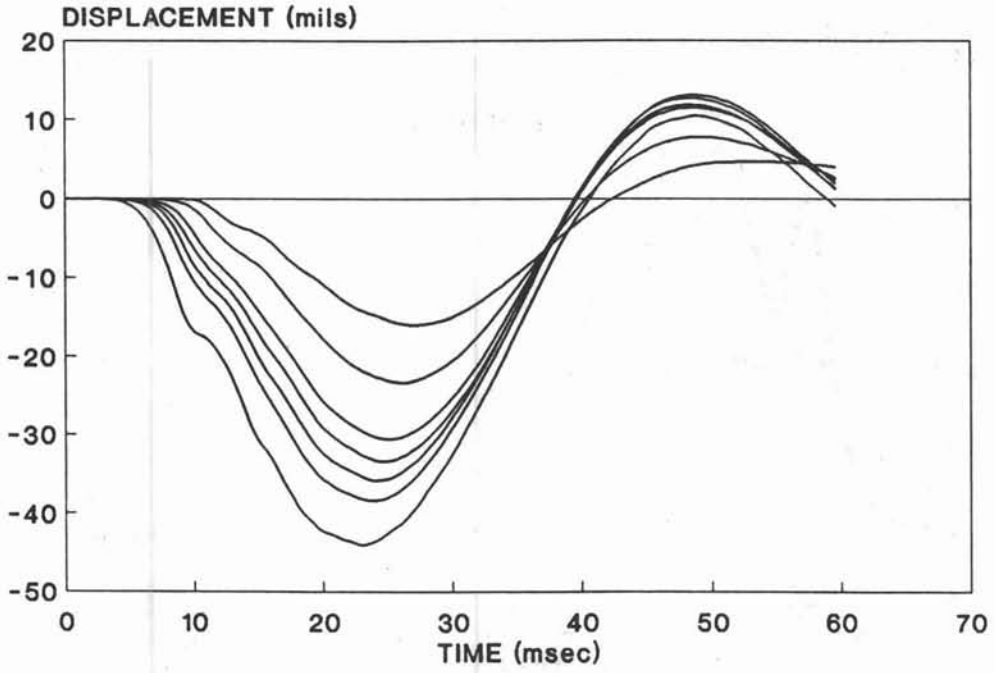

Figure 33
Displacement history for typical pile bent test.

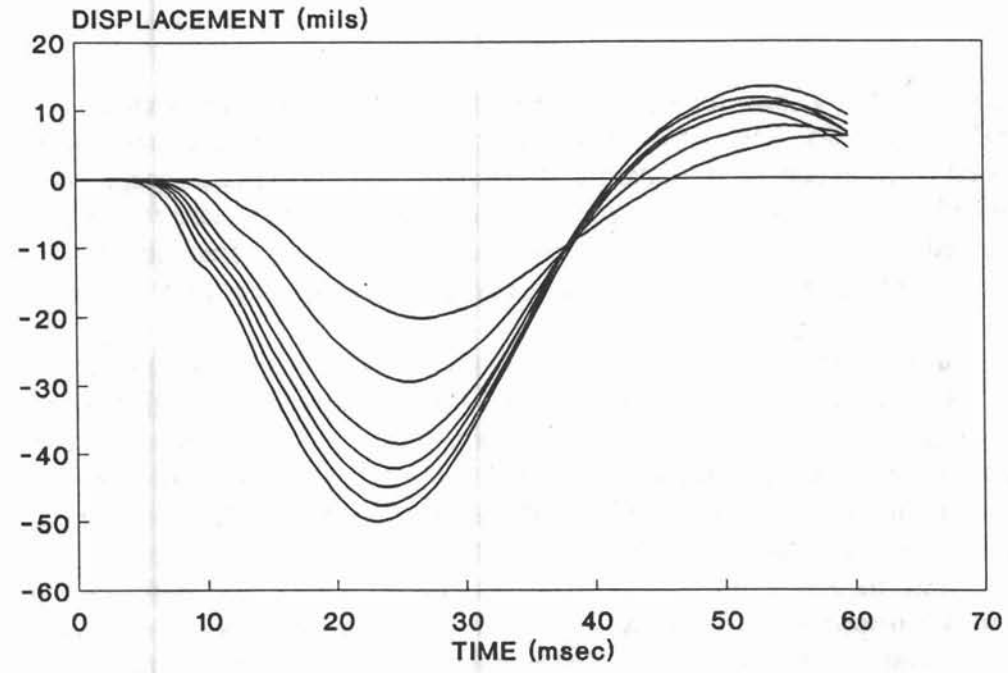

Figure 34
Displacement history for typical midspan test.

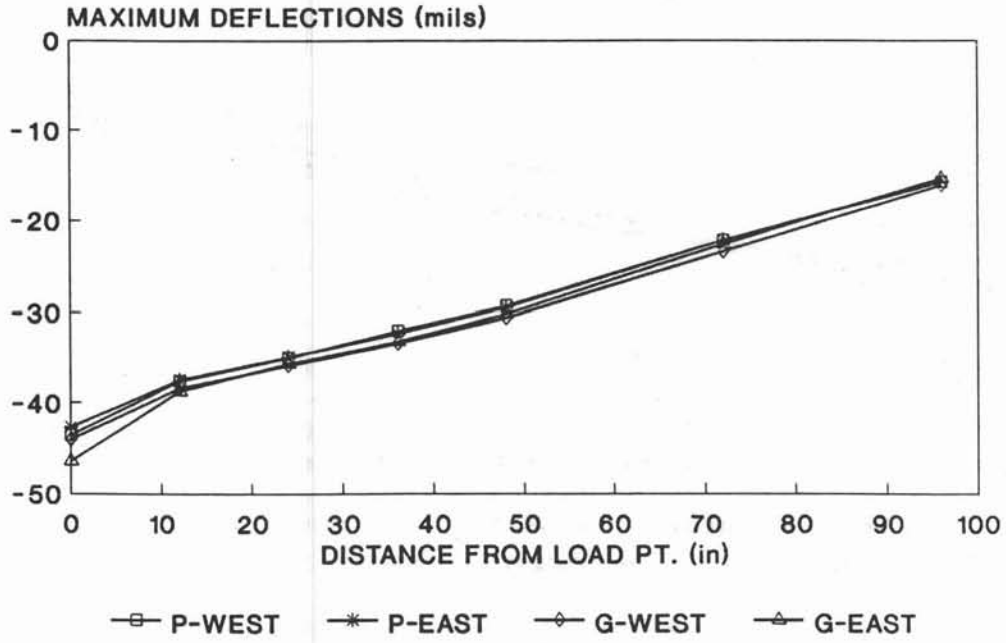

Figure 35
ILM results for pile bents P and G.

Both pile bents L and U had damage or deterioration on the east interior pile that resulted in a loss in the effective cross section of the member. Figure 36 compares the ILM results of these two pile bents with the results of pile bent P-West. The deflected shapes of the damaged bents were similar to P-West but the overall displacements increased by approximately 25 percent.

The visual inspection of spans RS and QR revealed no excess damage or deterioration and were the best condition for HB-4. This was reflected in the ILM results where displacements for spans RS and QR were among the smallest. Figure 37 shows the maximum deflection plots for these two spans. The maximum displacements occurring under the load were in the 50- to 60-mil range. The overall displacements of the midspan tests were approximately 28 percent greater than those at the pile bents reflecting the stiffness of the timber pile supports.

Figure 38 shows the influence of the damaged pile (pile bent L and U) on the midspan tests. The results of spans LM and TU are compared with RS-West from Figure 37. The displacements at spans LM and TU averaged 15 percent greater than the baseline results of RS-West. The ILM results indicated no major stiffness changes in the deck due to material damage of the deck. However, significant changes were detected due to rotted piles which provided no support to the bridge superstructure.

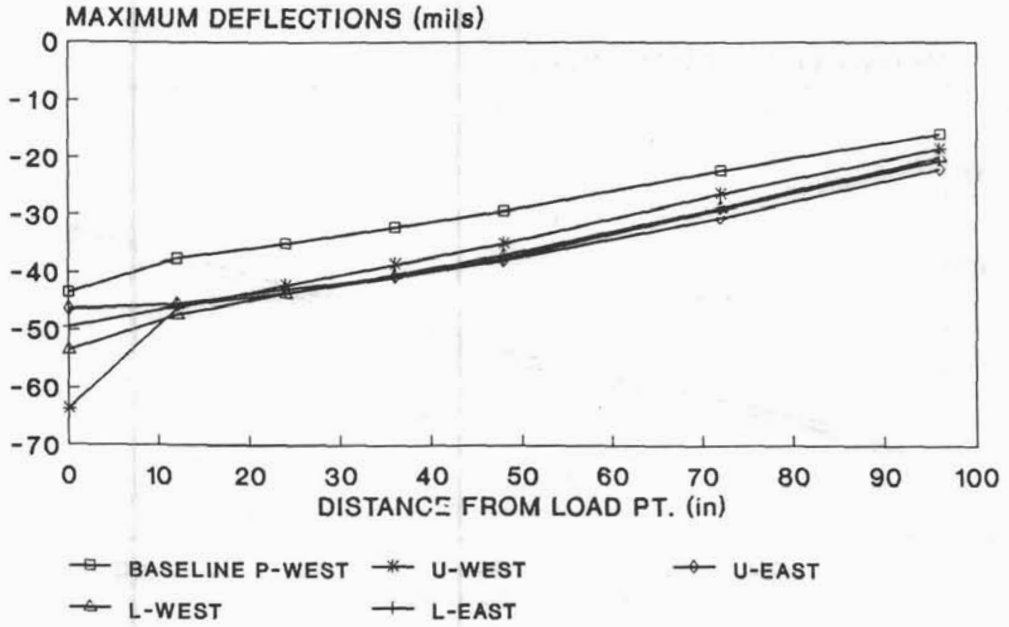

Figure 36
ILM results for pile bents L and U.

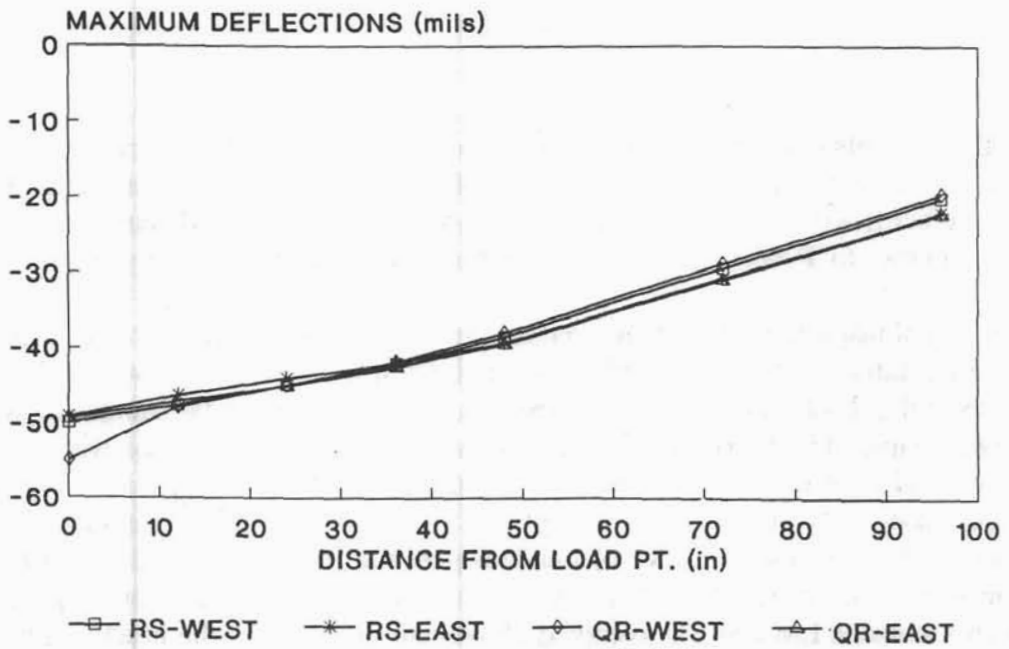

Figure 37
ILM results for spans QR and RS.

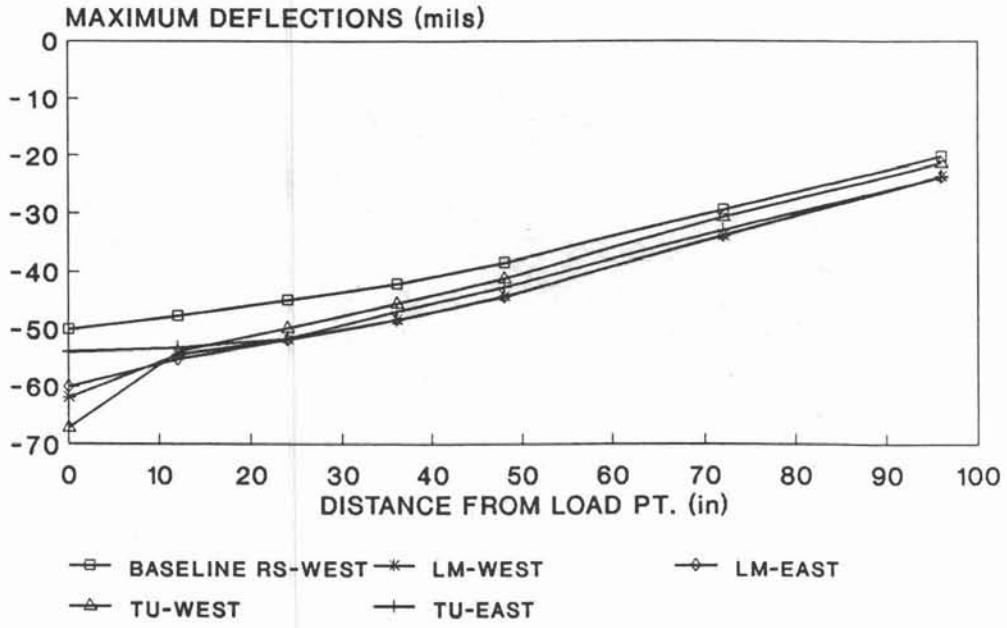

Figure 38
LM results for spans LM and TU.

Finite Element Analysis

A dynamic, linear, elastic finite element analysis was performed on HB-4 following the same methodology as that used on the model pier.

The bridge is divided into five sections which are separated by expansion joints in the deck. Each of these sections has eight spans. The finite element analysis was simplified by considering each eight-span section as an independent structure. Figure 39 shows the finite element mesh used in the analysis. By using symmetry, only four of the spans needed to be included in the model. Many Navy piers can be modeled in simplified fashion by making use of symmetry.

The deck was modeled using the same four node shell elements used on the model pier. These deck elements were 12 inches by 16 inches. The concrete guard rail beams were modeled using 12-inch-long beam elements. Since the centroid of the beams was not in the plane of the deck, the rigid link feature in the ADINA program was used to connect the beam nodes to the plate deck nodes (Ref 21). The piles were modeled using beam elements and the cross-bracing members were modeled using truss elements.

No core of coupon tests were performed to determine the material properties of the concrete and timber. Core tests on neighboring bridges yielded concrete strengths varying from 4,000 psi to 7,000 psi. Initial models used concrete strengths of 4,000 psi. The finite element model material properties were refined and calibrated by running a series of cases adjusting

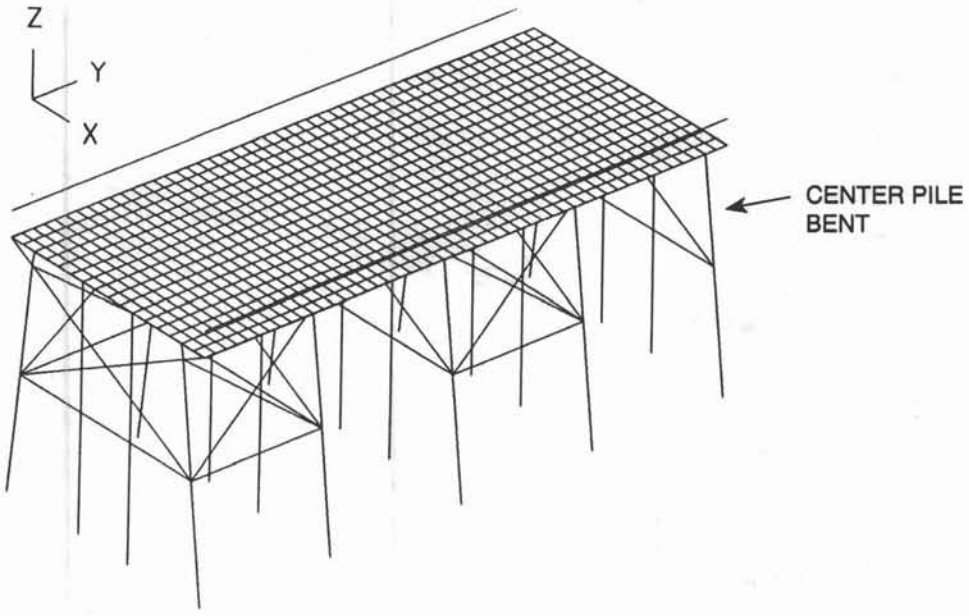

Figure 39
Finite element mesh of HB-4.

initial values for the elastic constants until the deflection responses corresponded with those of the experimental results for undamaged sections.

The orthotropic elements were used to model the deck. The orthotropic model was based on the transformed section properties in the two principle directions. Since the reinforcement in the top and bottom layers was the same throughout the structure, only one set of elastic constants was required. The undamaged material values for these constants determined from the calibration results are given in Table 8 (see Figure 39 for x and y orientation). The properties of the concrete side beams were based on the gross concrete section using an elastic modulus of 4,770 ksi. The properties of the timber piles and cross bracing were based on the nominal size of the member using an elastic modulus of 1,350 ksi.

Table 8
Elastic Constants for Orthotropic Model of HB-4 (ksi)

E_{xx}	E_{yy}	E_{xy}	G_{xy}	G_t
1,656	666	6,710	1,333	1,988

It is difficult to model pile-supported structures of this type because of the soil-pile interface. The length of piles supporting HB-4 was not known. It was assumed that a point on the pile 10 feet below the bottom cross bracing experienced negligible displacements and rotations. Thus, the piles of the finite element model were fixed in all degrees of freedom at this point.

Both symmetric and antisymmetric load cases were analyzed by changing the boundary conditions along the plane of symmetry for each case (Ref 29). For the symmetric case (loads along the center pile bent of the eight-span section), the y translations and x and z rotations were restrained along the center pile bent (see Figure 39). For the antisymmetric case, the x and z rotations and the y translations were restrained along the center pile bent.

Finite Element Model of Impact Load. The FWD was modeled using the method used on the pier model except only one truss member was used instead of six as shown in Figure 15. This was because the load plate covered a smaller area with respect to the deck element size. The total drop mass used was 3.98×10^{-3} kip-sec^2/in. (1,540 pounds). The equivalent stiffness determined experimentally for the 15.25-inch drop height and 1,540-pound combination was 60.0 kips/in.

When a symmetric load is applied to a symmetric model it is reduced by one-half and the displacements at each time step are equal to those experienced by the full structure. To determine the displacement response for an antisymmetric load case, the applied load must be reduced by one-half and applied to both the symmetric model and the antisymmetric model. The displacement results of these two models must be added together at each time step to determine the displacement history of the full structure with antisymmetric loading.

The force in the FWD spring at any time, t, defined by Equation 5 is as follows:

$$F(t) = (2\,g\,HMK)^{1/2} \sin \omega t$$

By substituting Equation 2 the above equation becomes:

$$F(t) = v_o\,(MK)^{1/2} \sin \omega t \qquad (13)$$

The force at any given time step is halved by simply substituting 1/2 v_o for v_o. The initial downward velocity used in the finite element analysis for the 15.25-inch drop height was 54.3 in./sec.

Undamaged Pile Results. The finite element model was calibrated by changing the stiffness properties of the deck and piles until the displacement results matched the measured values from undamaged pile bent P and G as well as undamaged spans QR and QS. The pile stiffnesses were calibrated by analyses of impact loads applied over the pile bent. After pile stiffnesses were determined, the deck elements were calibrated by considering the impact load applied at midspan. Figure 40 compares the maximum displacements of the calibrated finite element model with the ILM results of pile bent G and P. The finite element results closely matched the test results except for the region under the load. This is attributed to the compressed

asphalt layer (asphalt temperature was over 100°F during the ILM tests), which was not considered in the finite element analysis. Figure 41 compares the maximum displacement results of the finite element model to the ILM results of midspans QR and RS. Again, close agreement existed between the finite element and measured results.

Damaged Pile Results. Pile damage was modeled in the finite element analysis by reducing the cross-sectional area of each pile at the center pile bent to match the physical damage found in HB-4. The deck elements were not changed. The interior piles of bents L and U were providing no support and were subjects of this study. The load was applied at the pile bent and the area of the pile was reduced until the finite element displacements matched the experimental results. The results compared favorably when the cross-sectional area of the pile was reduced to approximately 10 percent of the original area. This was reasonable since the interior pile for bents L and U was rotted through the entire cross section. Figures 42 and 43 compare the finite element results with the ILM results of pile bents L and U for the east and west sides, respectively. The results closely match the measured results for both the east and west sides except for the compressed asphalt area under the load.

The influence of the damaged pile on the case of impact load applied at midspan was examined by using the same damaged model. The load was applied at the center of the adjacent span with no further parameter adjustment. Figures 44 and 45 compare these finite element results with the ILM results of the spans adjacent to the damaged pile, LM and TU. The results compare favorably for both of the east side tests shown in Figure 44 and for the west side LM test.

Parameter Sensitivity Analysis

Pile Support. Using the same method as on the pier finite element model, a parameter sensitivity analysis was performed to investigate the influence of pile deterioration on ILM response. Three cases were considered. In the first case, the load point was located over the pile bent at the usual position 1 foot from the center line and the cross-sectional area of an interior pile was reduced in increments of 25 percent of the original area (100, 75, 50, 25, 0). The second case applied the same procedure to the exterior pile. In the third case, the load point was located directly over an interior pile and the area of that pile was reduced for each run.

Figure 46 shows the results of the case in which the area of the interior pile was reduced and the load point was located 1 foot from the center line. The response in which the area of the pile was reduced to 10 percent is also plotted. The graphs show that small changes in the displacements occurred when the area of the pile was at least 25 percent of the original area. This reflected the structure's capacity to redistribute the load. Larger changes occurred when the area of the pile was reduced to 10 percent or the pile was eliminated (0 percent).

Figure 47 shows the results of the case in which the area of the exterior pile was reduced and the load point was located 1 foot from the center line. The graphs show that only small changes in the displacements occurred. It is questionable that these small differences could be discerned in ILM testing under field conditions encountered at HB-4.

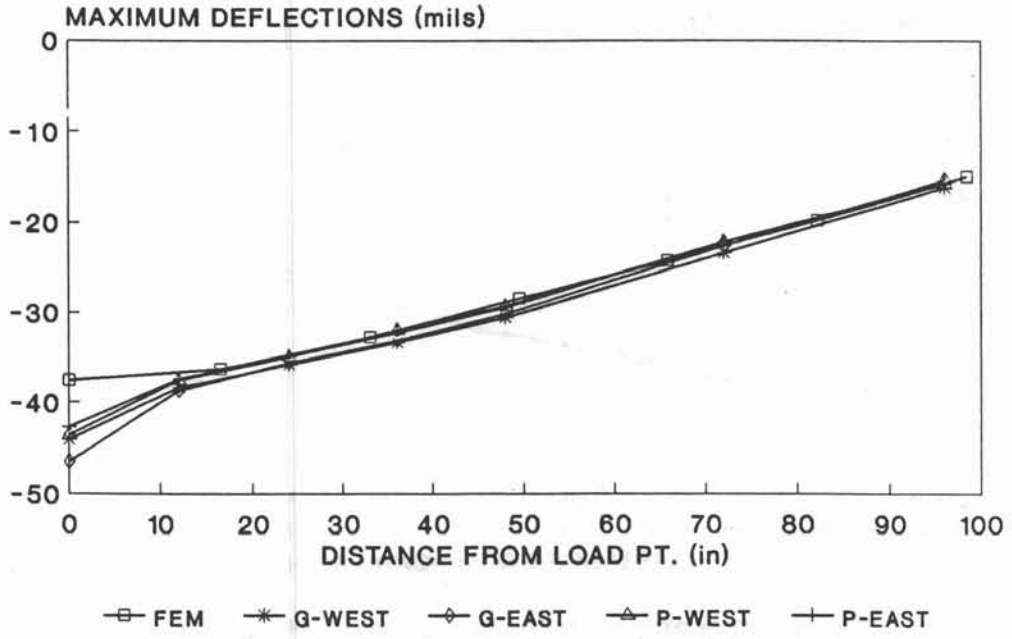

Figure 40
Finite element and ILM results for undamaged pile bent.

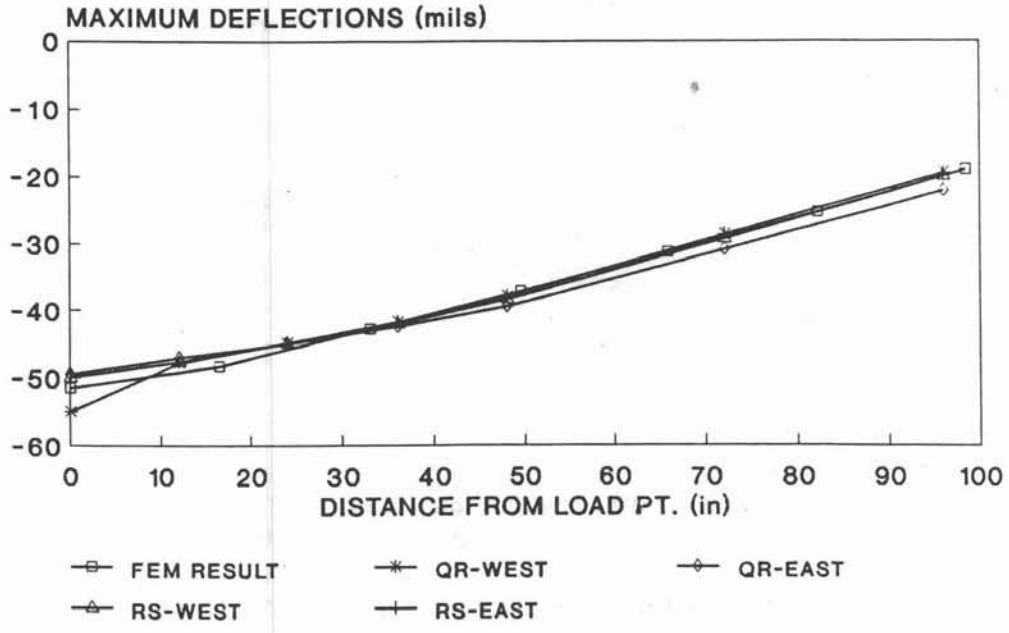

Figure 41
Finite element and ILM results for undamaged span.

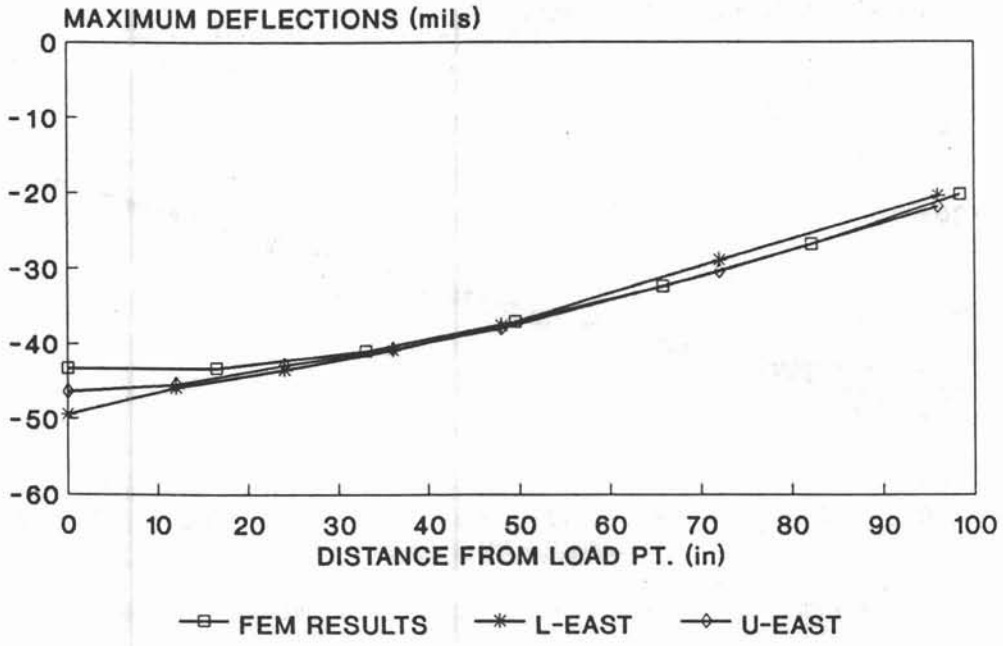

Figure 42
Finite element and ILM results for damaged pile, East side pile bent test.

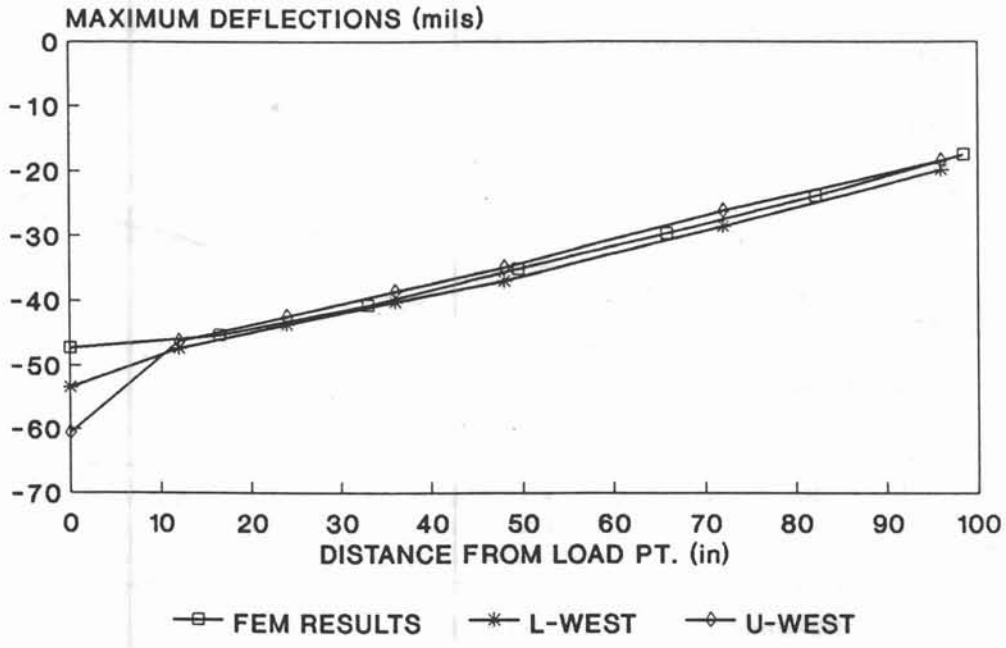

Figure 43
Finite element and ILM results for damaged pile, West side pile bent test.

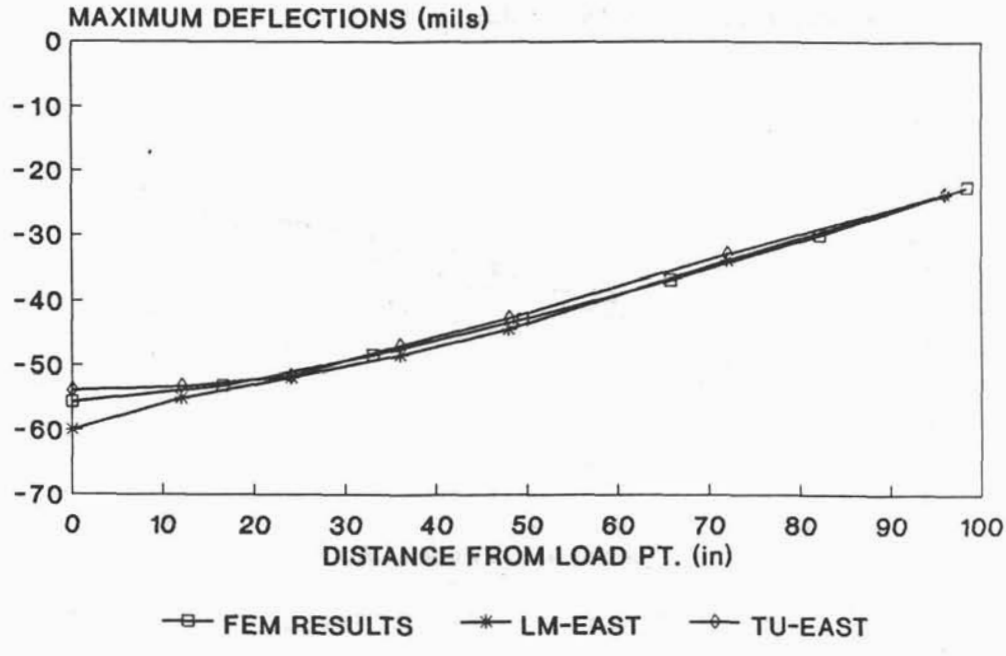

Figure 45
Finite element and ILM results for damaged pile, West side midspan test.

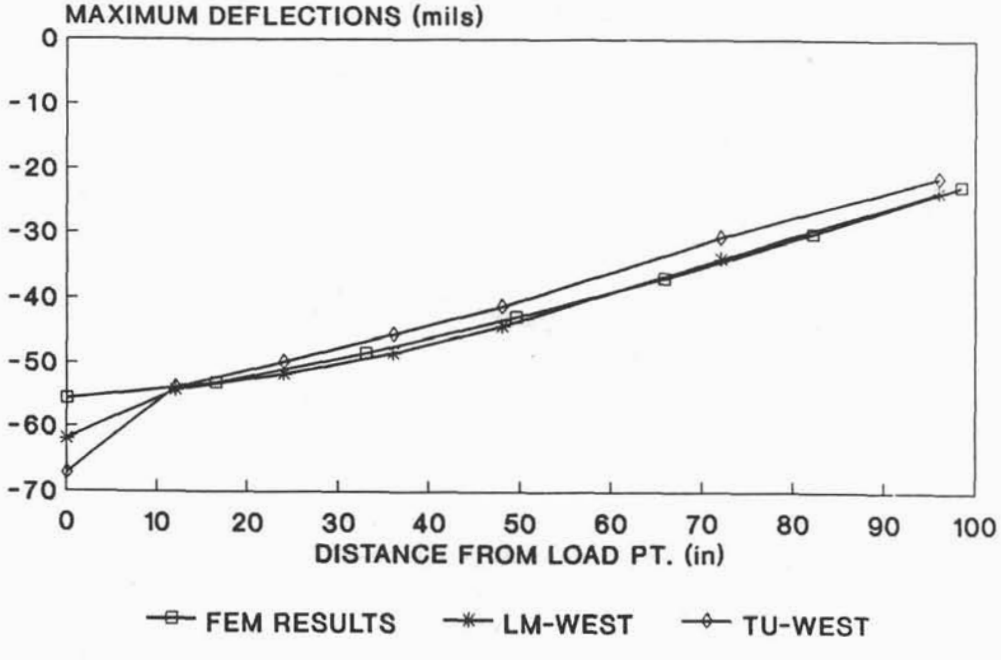

Figure 44
Finite element and ILM results for damaged pile, East side midspan test.

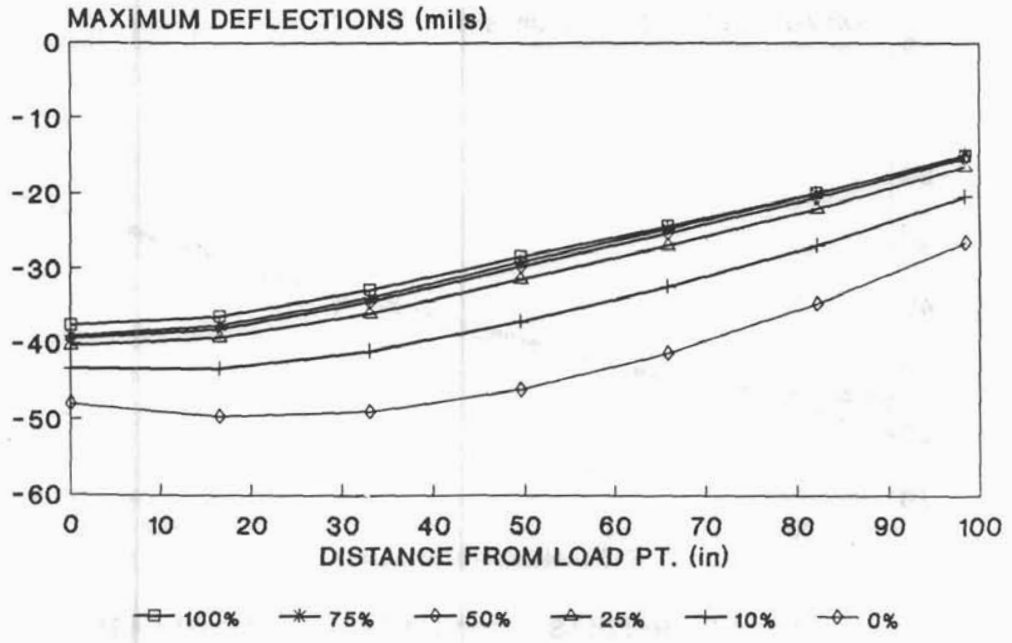

Figure 46
Results of sensitivity analysis, interior pile reduced,
load point at center.

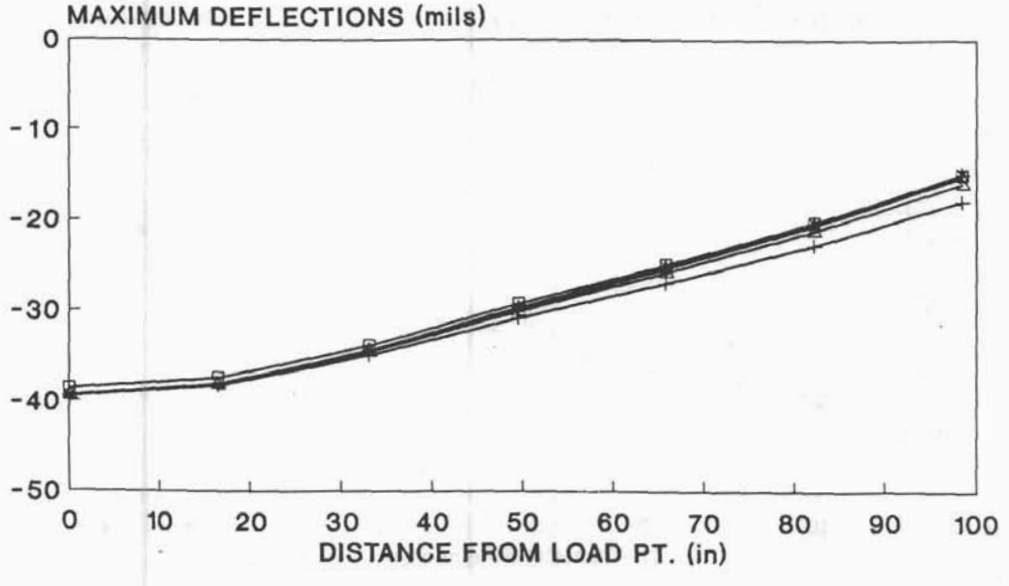

Figure 47
Results of sensitivity analysis, exterior pile reduced,
load point at center.

Figure 48 shows the results of the case in which the area of the interior pile was reduced and the load point was located directly over the pile. Again, small changes in the displacements occurred when the area of the pile was at least 25 percent of the original and probably could not be detected in field tests. An increase in displacements occurred only when the pile was eliminated. Small changes are a reflection of the structure's ability to redistribute internal forces in the vicinity of a damaged pile and also bridge deck stiffness. The loss of an internal pile resulted in only a 20 percent increase in flexure in the deck elements above the missing pile.

Imperceptible changes in response occur due to pile loss when the impact load is applied at midspan between pile bents. These changes could not usually be detected by the ILM process.

In applying the ILM procedure, test points over pile bents should be used to locate loss of pile support. Midspan test points will not locate weak piles. Test points should be as close as possible to pile supports. HB-4 can be surveyed along two lines passing midway between exterior and interior lines. Response will be sensitive to weak piles on either side of the point of impact load.

Deck Stiffness. The influence of reduced deck stiffness was investigated by reducing the deck element thickness over one span in 25 percent increments from the undamaged deck elements. Impact load was applied to the center line at the center pile bent in one case and to the midspan point of an adjacent span in another case. Results are presented in Figures 49 and 50. Response of 75 percent deck stiffness would not be perceptible from that of an undamaged deck by the ILM process. Midspan load points are best for detecting deck damage by the ILM process. Only small response differences were noted in the load case applied over the pile bent.

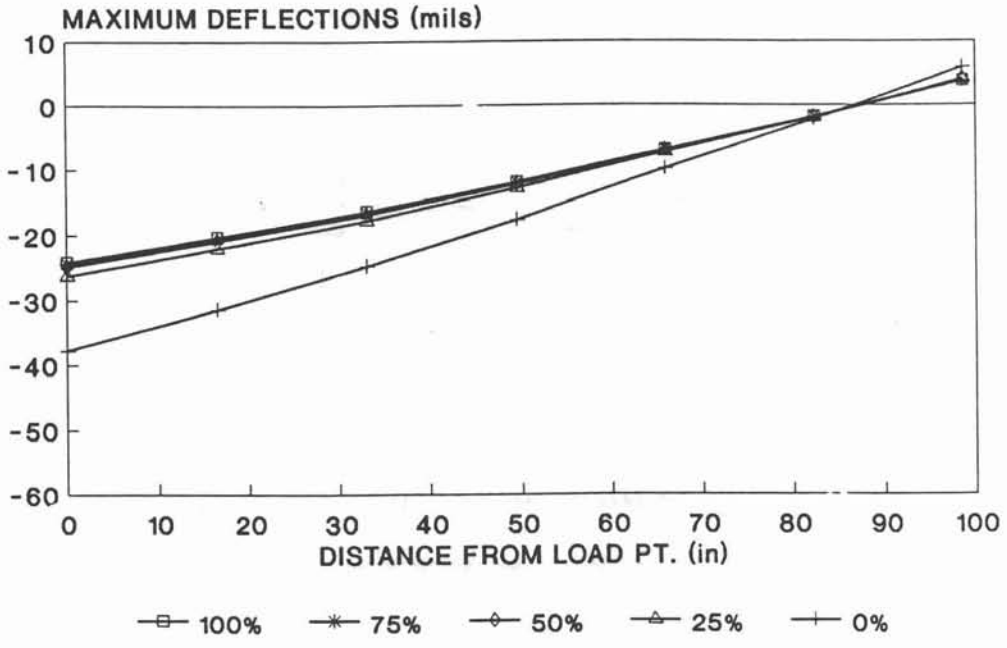

Figure 48
Results of sensitivity analysis, interior pile reduced, load point directly over pile.

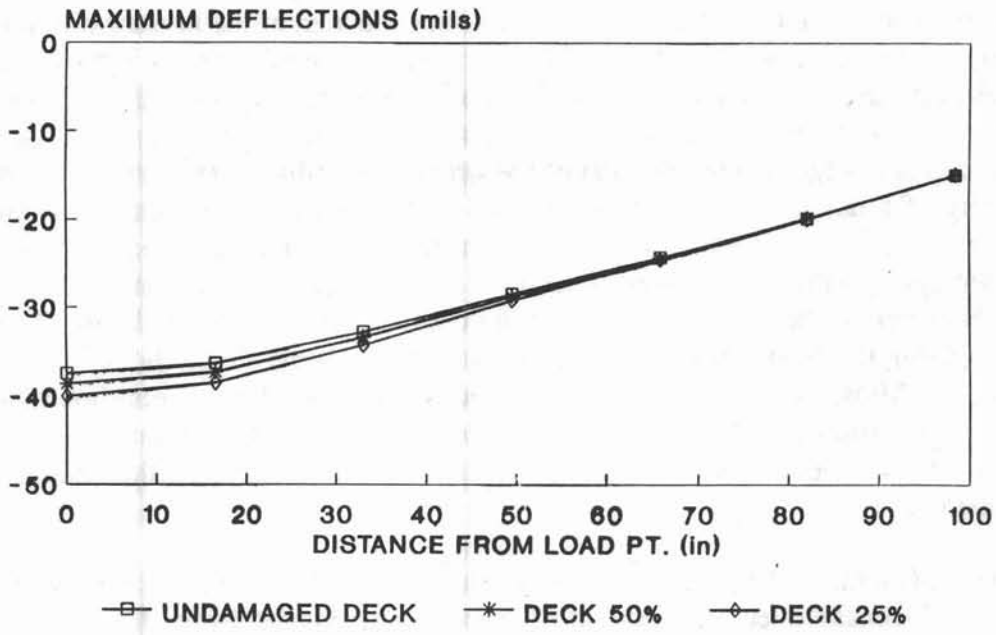

Figure 49
Simulated ILM response with loss of deck thickness and load applied over pile bent.

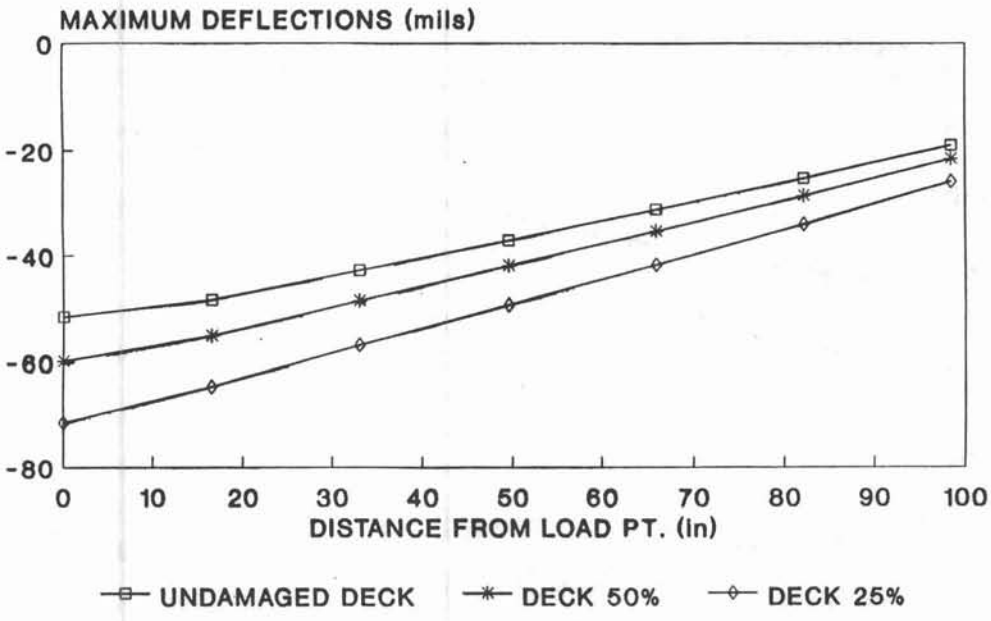

Figure 50
ILM response with loss of deck thickness and load applied at midspan between pile bents.

SUMMARY AND CONCLUSIONS

The impact load method was presented as a means of assessing the condition of pier and bridge structures. ILM tests were performed on a laboratory structure to investigate the sensitivity of the method in detecting stiffness changes that correlate to damage in the reinforced concrete deck. The method was successful in detecting the damage caused by overloading the deck slab. ILM tests were then performed on a full-scale structure to investigate the sensitivity of the method in detecting stiffness changes that correlate to pile deterioration. Again, the method was successful in detecting pile bents that had deteriorated piles.

The results of the ILM tests on undamaged areas of each structure were used to calibrate baseline finite element models. This calibration was performed by adjusting the elastic properties of the elements until the finite element results agreed with the experimental results. The FWD apparatus was represented in the finite element analysis by a single-degree-of-freedom (SDOF) mass-spring model consisting of truss elements and nodal masses. This simplified the input while still predicting accurate loads.

Two material models were evaluated in the finite element study: (1) an isotropic model based on the gross concrete section, and (2) an orthotropic model based on the transformed section in the two principle directions. The displaced shape of the orthotropic model matched the experimental results much closer than that of the isotropic model. Thus, the orthotropic model was used for both the pier and bridge analyses.

Using the baseline finite element models, damage sensitivity analyses were conducted. These models provided insight on the methodology's ability to detect and locate damage. The damage was represented by a reduction in the stiffness properties based on assumed section loss. The sensitivity analysis of the pier indicated that damaged areas as small as 4 square feet can be detected at distances up to 80 inches from the load point. The sensitivity analysis of the bridge indicated that pile deterioration can only be detected when the cross-section loss of the pile exceeds 75 percent. This reflected the redundancy inherent in this type of structure.

This study was limited to two specific cases. It is recommended that the research in this area be expanded to include the effects of two-way action in concrete decks and the sensitivity of other types of damage. It is also recommended that the effects of geometric parameters such as span length and pile configuration be examined and deck thickness be examined in more detail.

Finite elements will be further used to follow time-generated deterioration of the structure by periodic refinement to reflect changing response. The models also serve as a basis for setting load limits (rating) by setting thresholds for material deflection and/or stress values under service loads. The ILM equipment may cost as much as $120K. A 400-foot deck can be surveyed in 1 day. Initial finite element model development should take about 2 work weeks. Refinement and service load rating should require about 1 work month.

A pier condition assessment team can implement the ILM process by comparing the measured response with a baseline response stored in the computer that controls the FWD. Field operators can flag deviations for detailed inspection and further evaluation. For a given pier the team can develop the baseline response from a calibrated finite element model or from the FWD response on a known undamaged area. Finite element studies of the structure can help in establishing limiting variations from the baseline. These limits may be refined by correlating results to damage found by visual inspections. The finite element model of the actual structure can then be used to determine internal moments and to set load limits. These load limits will

be consistent with existing codes or design guidelines when the recommended load and material response factors are used in the finite element analysis.

REFERENCES

1. Transportation Research Board. National Cooperative Highway Research Program Report 312: Condition surveys of concrete bridge components - User's manual, by J. Minor, K.R. White, and R.S. Busch. Washington, DC, Dec 1988.

2. American Association of State Highway and Traffic Officials. Manual for maintenance inspection of bridges. Washington, DC, 1984.

3. American Society for Testing and Materials. Volume 4.2: Recommended practice for examination and sampling of hardened concrete in construction. Philadelphia, PA, 1986.

4. M. Sansalone and N.J. Carino. "Detecting delaminations in concrete slabs with and without overlays using the impact-echo method," American Concrete Institute Materials Journal, vol 86, no. 2, Mar-Apr 1989, pp 175-184.

5. T.R. Cantor. "Review of penetrating radar as applied to nondestructive evaluation of concrete," In-Situ/Nondestructive Testing on Concrete, SP-82, American Concrete Institute, Detroit, MI, 1984, pp 581-601.

6. D.E. Hudson. "Dynamic tests of full scale structures," Journal Mechanics Division, American Society of Civil Engineers, vol 103, no. EM6, Dec 1977, pp 1141-1157.

7. M. Biswas, A.K. Pandey, and M.M. Samman. "Diagnostic experimental spectral/modal analysis of a highway bridge," International Journal of Analytical and Experimental Modal Analysis, Jan 1989, pp 33-42.

8. Naval Facilities Engineering Command. Contract Report N47408-90-M-1154: Development of a numerical model, by N. Stubbs. Washington, DC, Jul 1990.

9. Naval Civil Engineering Laboratory. Memorandum to files on the identification of structural element stiffnesses of reinforced concrete decks from incomplete static test data, by M. Sanayei and S. Scampoli. Port Hueneme, CA, Sep 1989.

10. G.C. Hart and T.P. Yao. "System identification in structural dynamics," Journal Mechanics Division, American Society of Civil Engineers, vol 103, no. EM6, Dec 1977, pp 1089-1104.

11. Transporation Research Board. Analytical-empirical pavement evaluation using the falling weight deflectometer, by P. Ullidtz and R.N. Stubstad. Transportation Research Record 1022, Analysis and Testing of Granular Bases and Subbases. Washington, DC, 1985, pp 36-44.

12. Transportation Research Board. Transportation Research Circular, No. 189: An introduction to nondestructive structural evaluation of pavements, by W.M. Moore, D.I. Hanson, and J.W. Hall. Washington, DC, 1978.

13. _____. Concrete pavement joint stiffness evaluation, by J.M. Armaghani, J.M. Lybas, T. Mang, and B.E. Ruth. Transportation Research Record 1099, Concrete Pavement Design and Performance. Washington, DC, 1986, pp 22-36.

14. T. Krauthammer and L. Palmieri. "Concrete interface shear vibration spectroscopy," Journal of Engineering Mechanics, American Society of Civil Engineers, vol 117, no. 10, Oct 1991, pp 2251-2264.

15. Transportation Research Board. Dynamic analysis of falling weight deflectometer data, by B.E. Sebaaly, M.S. Mamlouk, and T.G. Davies. Transportation Research Record 1070, Pavement Response, Evaluation, and Data Collection. Washington, DC, 1986, pp 63-68.

16. J. Uzan and R.L. Lytton. "Analysis of pressure distribution under falling weight deflectometer loading," Journal of Transportation Engineers, American Society of Civil Engineers, vol 116, no. 2, Mar-Apr 1990, pp 246-250.

17. Naval Civil Engineering Laboratory. Technical Report R-935: Lateral load distribution in one-way flat slabs, by G.E. Warren and L.J. Malvar. Port Hueneme, CA, May 1991.

18. American Society of Testing and Materials. Volume 4.02: Annual book of ASTM standards, Concrete and aggregates. Philadelphia, PA, 1987.

19. _____. Volume 1.04: Annual book of ASTM standards, Steel-structural, reinforcing, pressure vessel, railway. Philadelphia, PA, 1987.

20. ADINA R&D, Inc. Report ARD 87-8: ADINA theory and modeling guide. Watertown, MA, Dec 1987.

21. _____. Report ARD 87-1: ADINA user's manual. Watertown, MA, Dec 1987.

22. K.J. Bathe. Finite element procedures in civil engineering. Englewood Cliffs, NJ, Prentice-Hall, Inc., 1982.

23. N.M. Newmark. "A method of computation for structural dynamics," American Society of Civil Engineers, vol 127, Part 1, 1962, pp 1406-1435.

24. B.E. Sebaaly, T.G. Davis, and M.S. Mamlouk. "Dynamics of falling weight deflectometer," Journal Transportation Division, American Society of Civil Engineers, vol 111, no. 6, Nov 1985.

25. D.E. Branson. "Deflections of reinforced concrete flexural members," Journal, American Concrete Institute, vol 63, no. 6, Jun 1966, pp 637-674.

26. P.K.K. Lee, D. Ho, and H.W. Chung. "Static and dynamic tests of concrete bridge," Journal Structures Division, American Society of Civil Engineers, vol 113, no. 1, Jan 1987, pp 61-73.

27. S. Timoshenko and S. Woinowsky-Krieger. Theory of plates and shells. New York, NY, McGraw-Hill, 1959.

28. Naval Civil Engineering Laboratory. Memorandum to files on the condition assessment of bridges HB-2, HB-2a, and HB-4 at Naval Weapons Station Earle, NJ, by G.E. Warren. Port Hueneme, CA, Jun 1990.

29. W. Weaver and J.M. Gere. Matrix analysis of framed structures, 2nd ed. New York, NY, Van Nostrand Reinhold, 1980.

DISTRIBUTION LIST

AFB / HQ TAC/DEMM (POLLARD), LANGLEY AFB, VA
AFESC / TIC LIB, TYNDALL AFB, FL
AMERICAN CONCRETE / LIB, DETROIT, MI
ARMY / R&D LAB, STRNC-UE, NATICK, MA
ARMY CECOM R&D TECH LIBRARY / ASNC-ELC-I-T, FT MONMOUTH, NJ
ARMY CERL / LIB, CHAMPAIGN, IL
ARMY ENGRG DIST / CENPS-ED-SD, SEATTLE, WA; LIB, SEATTLE, WA; PHILA, LIB, PHILADELPHIA, PA; CEHND-ED-CS, HUNTSVILLE, AL
ARMY EWES / CEWES-CD-P VICKSBURG, MS; LIB, VICKSBURG, MS; WESCD-P (MELBY), VICKSBURG, MS
ARMY MISSILE R&D CMD / CH, DOCS, SCI INFO CTR, REDSTONE ARSENAL, AL
ARMY MMRC / DRXMR-SM (LENOE), WATERTOWN, MA
ARVID GRANT & ASSOC / OLYMPIA, WA
ATLANTIC RICHFIELD CO / RE SMITH, DALLAS, TX
BATTELLE / D. FRINK, COLUMBUX, OH
BETHLEHEM STEEL CO / ENGRG DEPT, BETHLEHEM, PA
BLAKE, KIM / MARTINEZ, CA
BRITISH EMBASSY / SCI & TECH DEPT (WILKINS), WASHINGTON, DC
BROWN & ROOT / WARD, HOUSTON, TX
BROWN, ROBERT / TUSCALOOSA, AL
BULLOCK, TE / LA CANADA, CA
CASE WESTERN RESERVE UNIV / CE DEPT (PERDIKARIS), CLEVELAND, OH
CBC / CODE 155, PORT HUENEME, CA
CECOS / CODE C35, PORT HUENEME, CA
CHAO, JC / HOUSTON, TX
CHEE, WINSTON / GRETNA, LA
CHILDS ENGRG CORP / K.M. CHILDS, JR., MEDFIELD, MA
CITY OF LIVERMORE / DACKINS, PE, LIVERMORE, CA
CLARK, T. / SAN MATEO, CA
CLARKSON COLL OF TECH / CE DEPT, POTSDAM, NY
COGUARD R&D CEN / LIB, GROTON, CT
COLLEGE OF ENGINEERING / CE DEPT (GRACE), SOUTHFIELD, MI
COLORADO STATE UNIV / CE DEPT (CRISWELL), FT COLLINS, CO
COMCBLANT / CODE S3T, NORFOLK, VA
CONRAD ASSOC / LUISONI, VAN NUYS, CA
CONSOER TOWNSEND & ASSOC / SCHRAMM, CHICAGO, IL
CONSTRUCTION TECH LABS, INC / G. CORLEY, SKOKIE, IL
CORNELL UNIV / CIVIL & ENVIRON ENGRG, ITHACA, NY
DAMES & MOORE / LIB, LOS ANGELES, CA
DAVY DRAVO / WRIGHT, PITTSBURG, PA
DIA / DB-6E1, WASHINGTON, DC; DB-6E2, WASHINGTON, DC; VP-TPO, WASHINGTON, DC
DTRCEN / CODE 172, BETHESDA, MD
EDWARD K. NODA & ASSOC / HONOLULU, HI
ENGINEERING DATA MANAGEMENT / RONALD W. ANTHONY, FORT COLLINS, CO
FLORIDA ATLANTIC UNIV / OCEAN ENGRG DEPT (SU), BOCA RATON, FL
FLORIDA INST OF TECH / CE DEPT (KALAJIAN), MELBOURNE, FL
GEORGIA INST OF TECH / CE SCHL (KAHN), ATLANTA, GA; CE SCHL (SWANGER), ATLANTA, GA; CE SCHL (ZURUCK), ATLANTA, GA

GIORDANO, A.J. / SEWELL, NJ
GRUMMAN AEROSPACE CORP / TECH INFO CTR, BETHPAGE, NY
HAN-PADRON ASSOCIATES / DENNIS PADRON, NEW YORK, NY
HARDY, S.P. / SAN RAMON, CA
HAYNES & ASSOC / H. HAYNES, PE, OAKLAND, CA
HEUZE, F / ALAMO, CA
HJ DEGENKOLB ASSOC / W. MURDOUGH, SAN FRANCISCO, CA
JOHN HOPKINS UNIV / CE DEPT, JONES, BALTIMORE, MD
JOHN J MC MULLEN ASSOC / LIB, NEW YORK, NY
KAISER PERMANENTE MEDCIAL CARE PROGRAM / OAKLAND, CA
LAWRENCE LIVERMORE NATL LAB / FJ TOKARZ, LIVERMORE, CA
LEO A DALY CO / HONOLULU, HI
LIN OFFSHORE ENGRG / P. CHOW, SAN FRANCISCO, CA
LONG BEACH PORT / ENGRG DIR (ALLEN), LONG BEACH, CA; ENGRG DIR (LIZZI), LONG BEACH, CA
MICHIGAN TECH UNIV / (LIGON), HOUGHTON, MI; CO DEPT (HAAS), HOUGHTON, MI
MT DAVISSON / CE, SAVOY, IL
NAS / CODE 421, SAN DIEGO, CA; MIRAMAR, PWO, SAN DIEGO, CA
NAVFAC / N62, ARGENTINA, NF, FPO AE,
NAVFACENGCOM / CODE 04A1D, ALEXANDRIA, VA; CODE 04A3, ALEXANDRIA, VA; CODE 07, ALEXANDRIA, VA; CODE 07M (GROSS), ALEXANDRIA, VA
NAVFACENGCOM CHESDIV / CODE 112.1, WASHINGTON, DC
NAVFACENGCOM SOUTHDIV / CODE 04A3, CHARLESTON, SC; CODE 102H, CHARLESTON, SC; CODE 4023 (RDL), CHARLESTON, SC
NAVMEDCOM / NWREG, FAC ENGR, PWD, OAKLAND, CA
NAVOCEANSYSCEN / CODE 9642B, SAN DIEGO, CA
NAVPGSCOL / PWO, MONTEREY, CA
NAVSHIPREFAC / LIB, FPO AP; SCE, FPO AP
NAVSHIPYD / CODE 244.13, LONG BEACH, CA; CODE 443, BREMERTON, WA; MARE IS, CODE 202.13, VALLEJO, CA; MARE IS, CODE 280, VALLEJO, CA; MARE IS, PWO, VALLEJO, CA; NORFOLK, CODE 380, PORTSMOUTH, VA; TECH LIB, PORTSMOUTH, NH
NAVSTA / CO, LONG BEACH, CA
NAVSTA / CODE N4214, MAYPORT, FL
NEW ZEALAND CONCRETE RSCH ASSN / LIB, PORIRUA,
NIEDORODA, AW / GAINESVILLE, FL
NORTHDIV CONTRACTS OFFICE / ROICC, COLTS NECK, NJ
NRL / CODE 2511, WASHINGTON, DC; CODE 4670, WASHINGTON, DC
NUHN & ASSOC / A.C. NUHN, WAYZATA, NM
NUSC DET / LIB, NEWPORT, RI
OICC / ENGR AND CONST DEPT, APO AE,
OREGON STATE UNIV / CE DEPT (HICKS), CORVALLIS, OR
PAYE-KOSANOWSKY, S / POND EDDY, NY
PENNSYLVANIA STATE UNIV / GOTOLSKI, UNIVERSITY PARK, PA; RSCH LAB, STATE COLLEGE, PA
PILE BUCK, INC / SMOOT, JUPITER, FL
PMB ENGRG / LUNDBERG, SAN FRANCISCO, CA
PMTC / CODE 1018, POINT MUGU, CA
PORTLAND CEMENT ASSOC / AE FIORATO, SKOKIE, IL
PORTLAND STATE UNIV / ENGRG DEPT (MIGLIORI), PORTLAND, OR
PURDUE UNIV / CE SCOL (LEONARDS), WEST LAFAYETTE, IN

PWC / CODE 1011, PEARL HARBOR, HI; CODE 102, OAKLAND, CA CODE 400, OAKLAND, CA; CODE 412, SAN DIEGO, CA; CODE 420, OAKLAND, CA; CODE 421 (KAYA), PEARL HARBOR, HI; CODE 421 (QUIN), SAN DIEGO, CA; CODE 421 (REYNOLDS), SAN DIEGO, CA; CODE 421, NORFOLK, VA; CODE 422, SAN DIEGO, CA; CODE 423, SAN DIEGO, CA
SAN DIEGO PORT / PORT FAC, PROJ ENGR, SAN DIEGO, CA
SAN DIEGO STATE UNIV / CE DEPT (KRISHNAMOORTHY), SAN DIEGO, CA
SANDIA LABS / LIB, LIVERMORE, CA
SARGENT & HERKES, INC / JP PIERCE, JR, NEW ORLEANS, LA
SEATECH CORP / PERONI, MIAMI, FL
SEATTLE PORT / DAVE VAN VLEET, SEATTLE, WA
SEATTLE UNIV / CE DEPT (SCHWAEGLER), SEATTLE, WA
SHELL OIL CO / E. DOYLE, HOUSTON, TX
SIMPSON, GUMPERTZ & HEGER, INC / HILL, ARLINGTON, MA
SOUTHWEST RESEARCH INSTITUTE / THACKER, SAN ANTONIO, TX
SOUTHWEST RSCH INST / ENERGETIC SYS DEPT (ESPARZA), SAN ANTONIO, TX; KING, SAN ANTONIO, TX; M. POLCYN, SAN ANTONIO, TX; MARCHAND, SAN ANTONIO, TX
STATE UNIV OF NEW YORK / CE DEPT, BUFFALO, NY
TEXAS A&M UNIV / CE DEPT (MACHEMEHL), COLLEGE STATION, TX; CE DEPT (NIEDZWECKI); OCEAN ENGR PROJ, COLLEGE STATION, TX
TRW INC / ENGR LIB, CLEVELAND, OH
TUDOR ENGRG CO / ELLEGOOD, PHOENIX, AZ
UNIV OF CALIFORNIA / CE DEPT (FENVEX), BERKELEY, CA; CE DEPT (FOURNEY), LOS ANGELES, CA; CE DEPT (GERWICK), BERKELEY, CA; CE DEPT (TAYLOR), DAVIS, CA; CE DEPT (WILLIAMSON), BERKELEY, CA; NAVAL ARCHT DEPT, BERKELEY, CA
UNIV OF HAWAII / CE DEPT (CHIU), HONOLULU, HI; MANOA, LIB, HONOLULU, HI; OCEAN ENGRG DEPT (ERTEKIN), HONOLULU, HI; RIGGS, HONOLULU, HI
UNIV OF ILLINOIS / METZ REF RM, URBANA, IL
UNIV OF MICHIGAN / CE DEPT (RICHART), ANN ARBOR, MI
UNIV OF NEW MEXICO / NMERI (BEAN), ALBUQUERQUE, NM
UNIV OF RHODE ISLAND / CE DEPT (KOVACS), KINGSTON, RI; CE DEPT, KINGSTON, RI
UNIV OF TEXAS / CE DEPT (THOMPSON), AUSTIN, TX; CONSTRUCTION INDUSTRY INST, AUSTIN, TX; ECJ 4.8 (BREEN), AUSTIN, TX
UNIV OF WASHINGTON / CE DEPT (MATTOCK), SEATTLE, WA
UNIV OF WISCONSIN / GREAT LAKES STUDIES CEN, MILWAUKEE, WI
USDA / FOR SVC, REG BRIDGE ENGR, ALOHA, OR
USNA / CH, MECH ENGRG DEPT (C WU), ANNAPOLIS, MD; PWO, ANNAPOLIS, MD
VALLEY FORGE CORPORATE CENTER / FRANKLIN RESEARCH CENTER, NORRISTOWN, PA
VAN ALLEN, B / KINGSTON, NY
VSE / OCEAN ENGRG GROUP (MURTON), ALEXANDRIA, VA
VULCAN IRON WORKS, INC / DC WARRINGTON, CLEVELAND, TN
WESTINGHOUSE ELECTRIC CORP / LIB, PITTSBURG, PA
WISS, JANNEY, ELSTNER, & ASSOC / DW PFEIFER, NORTHBROOK, IL
WOODWARD-CLYDE CONSULTANTS / WEST REG, LIB, OAKLAND, CA